Description du Schema de Neige ISBA-ES (Explicit Snow)

Aaron Boone

April, 2002

Centre National de Recherches Météorologiques,Météo-France

42, avenue G. Coriolis, 31057 TOULOUSE Cedex France

TABLE OF CONTENTS

LIST OF ACRONYMS

CEN	Centre d'Etudes de la Neige (Center for Snow Studies)
CNRM	Centre Nationale Recherches Météorologiques (National Center for Meteorological Research)
CROCUS	Modèle d'évolution du manteaux neigeux du CEN (CEN snow model)
FSCA	Fractional Snow Covered Area
GCM	Global Climate Model
ISBA	Interaction Sol-Biosphère-Atmosphère (Interactions between Soil-Biosphere-Atmosphere)
ISBA-ES	Interaction Sol-Biosphère-Atmosphère-neige explicite (Interactions between Soil-Biosphere-Atmosphere Explicit Snow)
LWC	Liquid Water Content
SVAT	Soil Vegetation Atmosphere Transfer
SWE	Snow Water Equivalent

CHAPTER 1

ISBA-ES GENERAL DESCRIPTION

The Interactions between Soil Biosphere Atmosphere- Explicit Snow (ISBA-ES) scheme is a one-dimensional snow column model. The purpose of the new scheme is for use in local scale simulations alone or coupled to a SVAT, coupled SVAT (Soil Vegetation Atmosphere Transfer)-hydrological model applications, and coupling with atmospheric models. The model is based on similar such schemes described by Kondo and Yamazaki (1990), Loth et al. (1993), Lynch-Stieglitz (1994), and Sun et al. (1999), of which the latter three are designed for use in atmospheric climate models. Also, many aspects of the detailed snow scheme CROCUS (Brun et al. 1989; Brun et al. 1992) have been incorporated into the model in a simplified form. Simulation results and descriptions of testing can be found in Boone (2000), and Boone and Etchevers (2001).

ISBA-ES is coupled to the ISBA land surface scheme (Noilhan and Planton 1989; Noilhan and Mahfouf 1996) and is currently treated as a model option. The surface energy budget, atmospheric flux parameterizations and basic physics (such as thermodynamic calculations etc.) are taken directly from ISBA code/formulations. Some snow parameterizations (eg. albedo, snow fractional coverage, etc.) are also taken from the baseline Force-Restore ISBA snow scheme (Douville et al. 1995). In addition, the scheme has adopted some features of the detailed research and operational avalanche prediction model CROCUS (Brun et al. 1989; Brun et al. 1992). The model can be run/ has been tested for time steps up to approximately 30 minutes, although it is usually run coupled to ISBA in off-line

mode (not coupled to an atmospheric model) using 5 minute time steps. There are three variables saved each time step which are used to describe the state of the snow for three layers: the heat content (or specific enthalpy or the energy required to melt the snow), the snow density, and thickness. Snow surface albedo serves as a fourth prognostic variable (for just the uppermost layer). The model conserves both mass and energy to a high degree of accuracy.

ISBA-ES is written in FORTRAN90 and can be run for multiple points simultaneously (i.e. the code is vectorized). It has been compiled and tested on the Fujitzu Vector Processor and on an HP workstation at Météo-France. It has been evaluated at the local scale (Boone 2000, Boone and Etchevers 2001), and over a regional scale basin (Rhône) in France (Boone 2000) in off-line mode (i.e. using prescribed atmospheric forcing as opposed to being coupled with an atmospheric model) coupled to ISBA and the MODCOU distributed hydrological model (Girard 1974; Ledoux et al. 1989) for multiple annual cycles. It was also used in off-line mode for an Artic river basin under the auspices of the Project for the Intercomparison of Land-atmosphere Parameterization Schemes Phase 2-e (PILPS-2e: Bowling et al. 2002; Nijssen et al. 2002). It is currently participating in the off-line local scale model intercomparison project SNOWMIP (Essery et al. 1999). A scalar FORTRAN77 version has been tested on the HP and on a PC running Linux. It can be run coupled to ISBA (and an atmospheric model) or alone (using the same routine, with a different driver). In addition, there is a model option for coupling with either the standard ISBA Force-Restore module (Noilhan and Planton 1989; Noilhan and Mahfouf 1996) or an explicit multi-layer diffusion model (described in Boone 2000 and Boone et al. 2000).

1. Snow scheme physics

a. Mass balance

The mass conservation equation for the total snowpack is expressed for ISBA-ES as

$$\frac{\partial W_s}{\partial t} = (P_n + P_{rn} - R_{l\,N} - E_n) \quad , \tag{1.1}$$

where W_s corresponds to the total snowpack SWE which can also simply be expressed as the product of the average snowpack density (ρ_s) and total snow depth (D_s). E_n represents the combined evaporation and sublimation rate, and P_n represents the snowfall rate. The rainfall rate is represented by P_{rn}, which is equivalent to

$$P_{rn} = p_n\, P_r \quad ,$$

where p_n represents the fractional snow covered area (FSCA), and P_r is the rain rate over the snow-free and snow covered portions of the grid box. P_{rn} represents the portion of the total rainfall that is intercepted by the snow surface while the remaining rainfall is assumed to be intercepted by the snow-free soil and vegetation surfaces. The snow-runoff rate ($R_{l\,N}$) is defined as the rate at which liquid water leaves the base of the snow cover. All rates are expressed in kg m^{-2} s^{-1}.

b. Snow layering

The number of layers in ISBA-ES is prescribed to be three which is considered to be the minimum number of layers required to adequately resolve the snow thermal gradients between the top and the base of the snow cover (Lynch-Stieglitz 1994; Sun et al. 1999). The total snow depth (m) is defined as

$$D_s = P_n\, \Delta t/\rho_{\rm new} + \sum_{i=1}^{N_s} D_{s\,i} \tag{1.2}$$

where the model time step is Δt, $\rho_{\rm new}$ is the density (kg m^{-3}) of the snowfall [see Eq. (B.2)]. The snow layer thicknesses for the uppermost two layers are defined

using a scheme which is similar to that of Lynch-Stieglitz (1994):

$$D_{s\,1} = \delta_D\, 0.25 D_s \;+\; (1-\delta_D)\, D_{s\,1\,\max} \tag{1.3}$$

$$D_{s\,2} = \delta_D\, 0.50 D_s \;+\; (1-\delta_D)\; [0.34\,(D_s - D_{s\,1\,\max}) \;+\; D_{s\,1\,\max}]$$

$$(D_{s\,2} \leq 10\, D_{s\,1}) \tag{1.4}$$

$$D_{s\,3} = D_s - D_{s\,1} - D_{s\,2} \tag{1.5}$$

The ratios of each layer to the total depth is constant for snow depths below 0.2 m ($\delta_D = 1$) with the highest vertical resolution at the top and base of the snowpack. The upper layer thickness becomes constant ($D_{s\,1\,\max}$) when the total depth exceeds 0.2 m ($\delta_D = 0$), and it is prescribed to be 0.05 m in order to resolve the diurnal cycle based on an assumed thermal damping depth of snow (Dickinson 1988). In addition, the second layer is limited at 0.5 m since vertical gradients of heat and density are likely to be largest near the snow surface. An example of the snow grid scheme is shown in Fig. 1.1. However, note that the code is written such that any number of layers can be used (≥ 3), although the grid layering scheme (above) would have to be modified accordingly by the user.

The vertical profiles of snow mass and heat are redistributed after the grid thicknesses have been updated in order to ensure mass and heat conservation. This implies a certain degree of mixing (of mass and heat) at layer interfaces during periods of snow melt and accumulation, so that layer "memory" can be relatively short under these circumstances for relatively thin layers. See Appendix B section 6 for details.

c. Density

All of the snow internal processes, such as absorption of incident solar radiation, liquid water retention, heat transfer and compaction, are parameterized as functions of snow density in ISBA-ES.

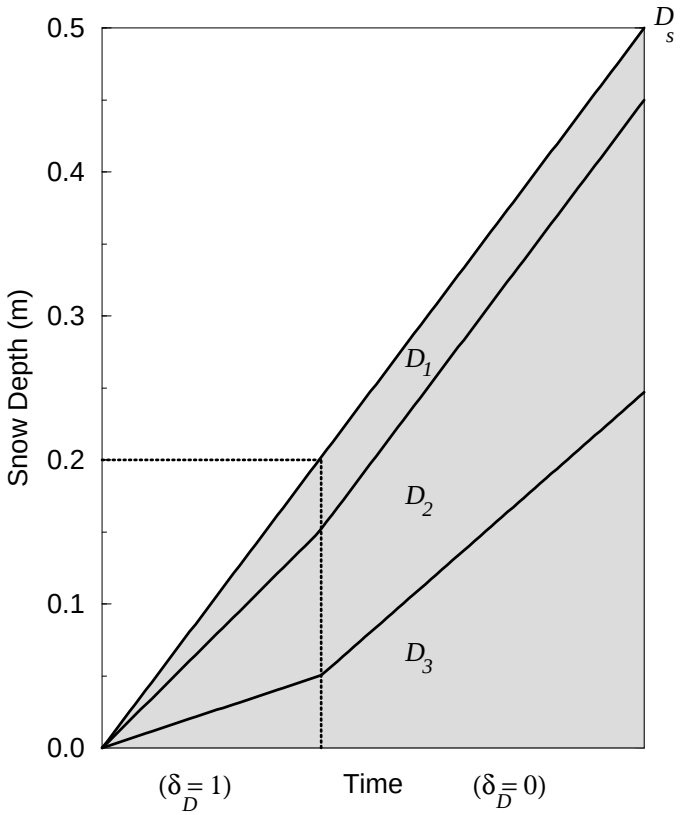

FIG. 1.1. An example of the snow grid evolution in time as a function of increasing total snow depth.

Snowfall usually has the effect of reducing the uppermost layer density. The snow density is updated using a simple thickness weighting scheme as

$$\rho_{s\,1}{}' = \frac{D_{s\,1}\rho_{s\,1} + P_n\,\Delta t}{D_{s\,1} + (P_n\,\Delta t/\rho_{\rm new})} \quad .$$

The local rate of change of density (increases) due to the weight of the overlying snow and settling (primarily of new snow) is parameterized following Anderson (1976) as

$$\frac{1}{\rho_{s\,i}}\frac{\partial \rho_{s\,i}}{\partial t} = \frac{\sigma_{s\,i}}{\eta_{s\,i}\,(T_{s\,i}, \rho_{s\,i})} + a_{sc}\exp\left[-b_{sc}\,(T_f - T_{s\,i}) - c_{sc}\max\left(0,\ \rho_{s\,i} - \rho_{sc}\right)\right] \quad (1.6)$$

where the first term on the right-hand side of Eq. (1.6) represents overburden (the compactive viscosity term, see Eq. B.1). The pressure of the overlying snow is represented by σ_s (Pa), and η_s is the snow viscosity (Pa s) which is an exponential function of snow temperature and density (Mellor 1964; Kojima 1967). The second term represents the thermal metamorphism (Anderson 1976) which can be significant for fresh relatively low-density snowfall. The values from Anderson (1976) are used: $a_{sc} = 2.8 \times 10^{-6}$ s^{-1}, $b_{sc} = 4.2 \times 10^{-2}$, K^{-1}, $c_{sc} = 460$ m^3 kg^{-1}, and $\rho_{sc} = 150$ kg m^{-3}. Note that the compaction constants can be treated as site-dependent calibration parameters, but they are held constant for all conditions and locations in the current model. This is also generally the case for snow model density parameters in SVATs intended for or coupled to GCMs (eg.s Pitman et al. 1991; Verseghy 1991; Lynch-Stieglitz 1994; Douville et al. 1995; Yang et al. 1997; Loth et al. 1998; Sud and Mocko 1999) and operational numerical weather prediction models (eg. Koren et al. 1999). This assumption is made because application in an atmospheric model would be difficult as large scale or global datasets of these parameters have not been established. After the newly settled/compacted snow density has been calculated, the layer thicknesses are proportionally decreased such that total mass is unchanged:

$$D'_{s\,i} = D_{s\,i}\,\rho_{s\,i}/\rho'_{s\,i} \ ,$$

where the $'$ indicates the updated value.

Both snow-settling schemes allow the snow to compact to densities of approximately 450 kg m^{-3}. Additional density increases in ISBA-ES arise from compaction due to melting, infiltration of rainwater and retention of snow melt (discussed in a subsequent section).

d. Energy balance and heat flow

The heat content or energy required to melt a snow layer for each snow layer is defined using an expression similar to that of Lynch-Stieglitz (1994) and Sun et al. (1999) as

$$H_{s\,i} = c_{s\,i}\, D_{s\,i}\, (T_{s\,i} - T_f) \;-\; L_f\, (W_{s\,i} - W_{l\,i}) \quad , \tag{1.7}$$

where L_f is the latent heat of fusion and H_s is express in J m^{-2}. The snow heat capacity is defined following Verseghy (1991) (Eq. B.3). The snow layer liquid water content (kg m^{-2}) is represented by W_l. The snow heat content is used in order to allow the presence of either cold (dry) or warm (wet) snow. The heat content is used to diagnose the snow temperature using Eq. (1.7) assuming that there is no liquid water in the snow layer ($W_l = 0$).

$$T_{s\,i} = T_f \;+\; (H_{s\,i} + L_f\, W_{s\,i}) \,/\, (c_{s\,i}\, D_{s\,i}) \qquad\qquad (W_{l\,i} = 0)$$

If the calculated temperature exceeds the freezing point, then the temperature is set to T_f and the liquid water content is diagnosed from Eq. (1.7):

$$W_{l\,i} = W_{s\,i} \;+\; (H_{s\,i}/L_f) \qquad\qquad (T_{s\,i} = T_f)$$

A similar procedure is used by Sun et al. (1999).

Snow heat flow is along the thermal gradient as any snow melt or percolated water within the snow cover is assumed to have zero heat content. In addition, solar radiation decays exponentially within the snowpack as a function depth. The layer-averaged snow temperature equation ($T_{s\,i}$) is then expressed as

$$c_{s\,i} D_{s\,i} \frac{\partial T_{s\,i}}{\partial t} = G_{s\,i-1} - G_{s\,i} - F_{s\,i} \quad , \tag{1.8}$$

where F_s represents latent heat absorption or release due to phase changes (between water and ice). The heat flux G_s is simply expressed as

$$G_{s\,i} = J_{s\,i} + Q_{s\,i} \tag{1.9}$$

where the heat conduction (J_s) and radiation (Q_s) flux terms are defined as

$$Q_{s\,i} = R_g\,(1-\alpha_n)\exp\left(-\nu_{s\,i}\,z_{s\,i}\right) \qquad (i = 0, N_s - 1) \tag{1.10}$$

$$J_{s\,i} = 2\,\overline{\Lambda}_{s\,i}\frac{(T_{s\,i} - T_{s\,i+1})}{(D_{s\,i} + D_{s\,i+1})} \qquad (i = 1, N_s - 1) \tag{1.11}$$

where

$$\overline{\Lambda}_{s\,i} = \frac{D_{s\,i}\Lambda_{s\,i} \;+\; D_{s\,i+1}\Lambda_{s\,i+1}}{D_{s\,i} + D_{s\,i+1}} \qquad (i = 1, N_s - 1) \tag{1.12}$$

$$z_{s\,i} = \sum_{j=1}^{i} D_{s\,j} \qquad (i = 1, N_s) \tag{1.13}$$

where the depth from the top of the snowpack (i.e. atmosphere/snow interface) to the base of layer i is given by $z_{s\,i}$. A schematic diagram for a N_s layer snowpack is shown in Fig. 1.2: mass sources/sinks/transfers are indicated using solid arrows, and solar radiation transmission and heat flux pathways are represented by hollow arrows. The layer-average state variables (which are saved at each time step) are enclosed inside of a rounded box within each snow layer, and layer-average diagnostic variables are enclosed within a dotted box. The shaded region represents the surface soil/vegetation layer. The symbols are defined in the text and in the List of Symbols in Appendix A.

Eq. (1.8) is solved assuming a minimum layer thickness of 0.01 m, even though the true total snow layer depth may be thinner. This is done to ensure numerical stability. For snow cover less than this threshold, the influence on the surface fluxes and near surface hydrology in ISBA is generally quite small so that this approximation is justified.

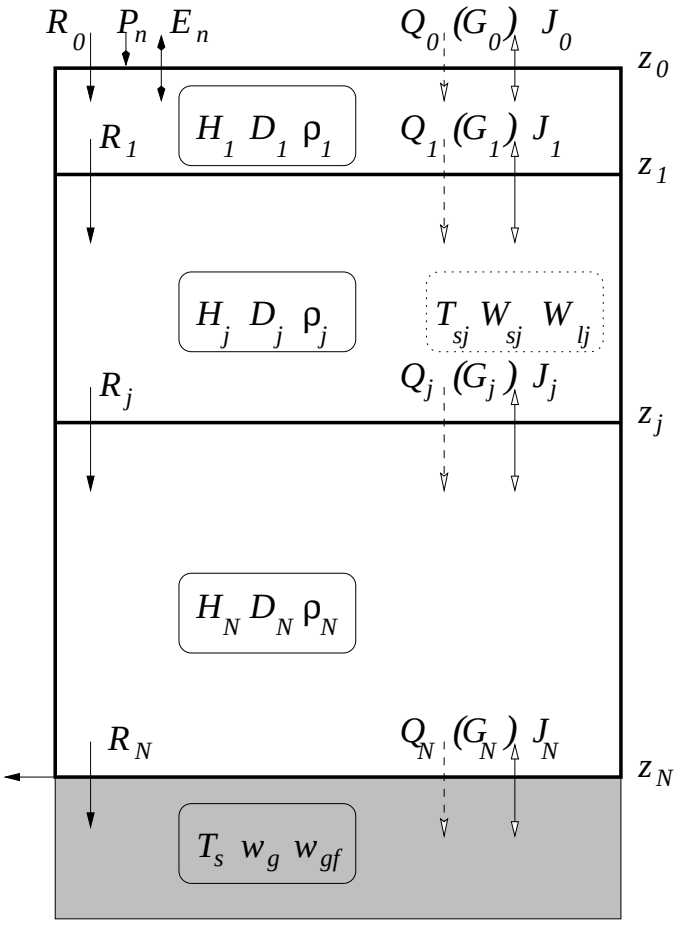

FIG. 1.2. Schematic diagram of the N_s-layer scheme. State variables (enclosed in rounded boxes) and mass (solid arrows) and energy pathways (hollow arrows) are indicated. The shaded region represents the surface soil/vegetation layer. The symbols are defined in the text and in Appendix A.

The snow thermal conductivity (Λ_s: W m^{-1} K^{-1}) increases quadratically as a function of increasing snow density (Anderson 1976: see Eq. B.4). There is an additional contribution due to vapor transfer in the snow which is especially important at low snow densities and high altitudes which is expressed following Sun et al. (1999). The heat flux at the snow/soil interface ($G_{s\,N}$) is described in the section on coupling with the SVAT scheme.

The incoming shortwave radiation (W m^{-2}) is represented by R_g and ν_s is the shortwave radiation extinction coefficient (Bohren and Barkstrom 1974). The snow

grain size is needed for this calculation and is parameterized following Anderson (1976) (see Eq. B.8). The snow surface albedo is modeled using time constants following Douville et al. (1995) (see Appendix B). A linear decrease rate is used for dry snow (Baker et al. 1990) and an exponential decrease rate is used to model the wet metamorphism (Verseghy 1991).

The net heat flux at the atmosphere/snow interface is expressed as

$$G_{s\,0} = (1 - \alpha_n)\, R_g + \epsilon_n \left(R_{at} - \sigma {T_{s\,1}}^4 \right) - H_n - LE_n + P_{rn}\, c_w\, (T_{a\,l} - T_f) \quad (1.14)$$

where R_{at} is the down-welling atmospheric longwave radiation, the snow emissivity (ϵ_n) is assumed to be 1 (for all three snow models) and σ represents the Stefan-Botzmann constant. The last term on the right hand side of Eq. (1.14) is a precipitation advection term where c_w represents the specific heat of water (4187 J kg^{-1} K^{-1}). The temperature of rainfall ($T_{a\,l}$) is simply assumed to be larger of T_a and T_f.

The snow surface flux terms ($G_{s\,0}$) are linearized with respect to the uppermost snow layer temperature using the same method as in ISBA (Giordani 1993). The solution procedure for the entire profile is fully implicit when no melting is occurring so that relatively large time steps may be used for thin snow cover depths. Note that during snow melt events, an explicit representation of the surface energy budget (i.e. a constant surface snow temperature at the freezing point) can produce significantly different surface fluxes from those obtained using an implicit (linearized) approach. When melting occurs in the surface layer for at least two consecutive time steps, the surface energy balance is solved using an explicit approach as the solution is exact and stable (as the surface temperature is constant at T_f). This method is adopted from CROCUS (Brun et al. 1992) (see Appendix D for details).

e. Surface turbulent fluxes

The latent heat flux from the snow includes contributions from evaporation of liquid water in the surface snow layer and sublimation and it is defined as

$$LE_n = [\chi_1 \, L_s \, + \, (1 - \chi_1) \, L_v] \, E_n = [\chi_1 \, L_f \, + \, L_v] \, E_n$$
$$E_n = \rho_a \, C_H \, V_a \, [q_{\rm sat} \, (T_{s\,1}) - q_a] \quad , \tag{1.15}$$

where L_v and L_s denote the latent heat of vaporization and sublimation, respectively ($L_s = L_f + L_v$). The fraction of the total mass of the surface layer which is frozen is represented by χ_1, which is defined for a snow layer as

$$\chi_i = 1 - (W_{l\,i}/W_{s\,i})$$

Evaporation is only possible when $T_{s\,1} = T_f$ and $W_{l\,1} > 0$. Atmospheric values for the air density, wind speed and specific humidity are represented by ρ_a, V_a, and q_a, respectively. Evaporation of liquid water reduces the mass in the uppermost snow layer while leaving the thickness unchanged. Sublimation, on the other hand, reduces mass by decreasing the thickness while leaving the density unchanged.

The sensible heat flux is

$$H_n = \rho_a \, C_p \, C_H \, V_a \, (T_{s\,1} - T_a) \quad , \tag{1.16}$$

where C_p is the specific heat of air. The turbulent exchange coefficient (C_H) relationship is the same as that used in ISBA-FR (Noilhan and Mahfouf 1996) which is based on the formulation by Louis (1979):

$$C_H = \left[\frac{k^2}{\ln (z_u/z_{0t}) \ln (z_a/z_{0t})} \right] \, f \, (R_i) \tag{1.17}$$

where z_u and z_a are the heights of the wind and air temperature measurements, respectively, and the von Karman constant is denoted by k. The transfer coefficient

C_H decreases as a function of increasing stability or R_i. The grid box effective surface roughness length (z_{0t}) takes into account the effects of both snow and vegetation (see Appendix E). The ISBA C_H coefficient is shown as a function of R_i in Fig. 1.3 for two standard values of z_u (2 and 10 m), $z_a = 2$ m, and for $z_{0t} = 10^{-3}$, 10^{-2} and 10^{-1} m. The C_H coefficient for CROCUS (used for an alpine site, see Martin and Lejeune 1998) has also been plotted as a reference.

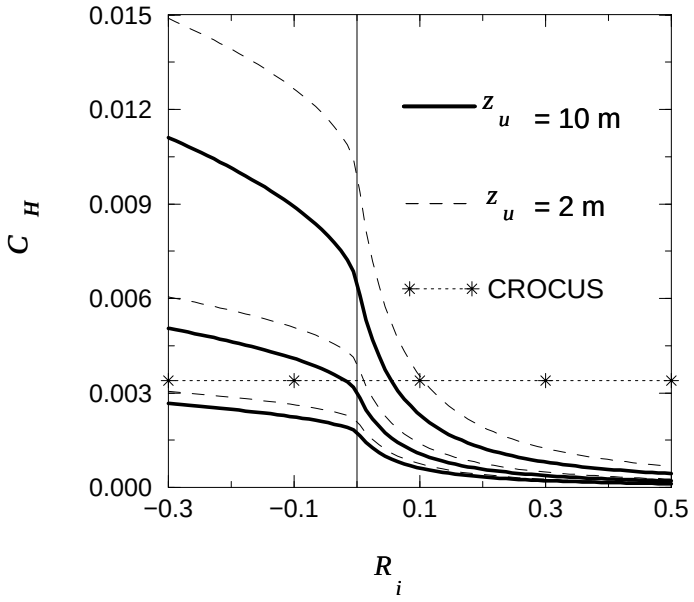

FIG. 1.3. The ISBA turbulent transfer coefficient (C_H) as a function of the bulk Richardson number (R_i) for two standard values of z_u (2 and 10 m) and $z_a = 2$ m. The C_H curves for three values of the surface roughness length are shown: $z_{0t} = 10^{-3}$, 10^{-2} and 10^{-1} m (C_H increases for larger z_{0t}). The C_H value for CROCUS is indicated.

It is known that the bulk-Richardson formulation generally under-predicts turbulent transfer for very stable conditions and small roughness lengths assumed to be typical of snow-covered surfaces (eg.s Hardy et al. 1997; Krinner et al. 1999; Derbyshire 1999; Jordan et al. 1999). In addition, Andreas (1996) gives a good discussion on the difficulty in parameterizing turbulent transfer over cold snow and

ice covered surfaces. ISBA-ES uses an effective roughness length which implicitly represents the effects of upstream roughness elements on the snow atmospheric surface layer. CROCUS uses the same basic expressions for H_n and LE, however it treats C_H as a site specific calibration parameter. In general, values on the order of 10^{-3} are used for mountainous sites as they have been shown to produce the best snow depth and temperature simulations compared to observations (Martin and Lejeune 1998). There are essentially four methods currently used by snow models; 1) define a critical $R_{i\,\max}$ above which C_H remains constant (eg.s 0.160, Hardy et al. 1997; 0.012, Martin and Lejeune 1998; 0.100, Krinner et al. 1999), 2) fix a minimum or constant C_H for stable conditions (eg.s $f\left(R_i > 0\right) = 1$, Jordan 1991; $C_H = 0.002$, Kondo and Yamazaki 1990), 3) modify the formulation of $C_H\left(R_i > 0\right)$ (Viterbo et al. 1999; Jordan et al. 1999), and 4) define an effective roughness length which implicitly represents the effects of upstream or pretruding roughness elements (which presumably are larger than roughness lengths for a flat surface) on the snow atmospheric surface layer (eg. for ISBA, Essery et al. 1999).

ISBA uses an effective snow surface roughness length (z_{0t}) which includes the influence of embedded or upstream roughness elements (such as relief or vegetation) for the case of a point or local scale, while for mesoscale or larger scale applications z_{0t} represents the grid box average roughness length of both snow covered and snow free surfaces. But, as Martin and Lejeune (1998) suggest, C_H values can, under certain conditions, still become quite low, thereby effectively decoupling (too much) the surface from the atmosphere. A model option exists which consists of the use of a maximum Richardson number ($R_{i\,\max}$). Currently, a cut-off value of 0.20 (similar to the value used in the operational numerical weather prediction version of ISBA) is used as this results in minimum C_H values on the order of 10^{-3} (the order of magnitude suggested in the aforementioned studies) for snow roughness

lengths ranging from approximately 10^{-3} to 10^{-1} m (see Marks and Winstral 2001 for a discussion on snow roughness length values quoted in the literature). The drawback of this method is that the model can be quite sensitive to the value of $R_{i\,\max}$ for relatively warm weather conditions. The problem of decoupling between the atmosphere and surface for extremely stable conditions is a fairly common problem among SVAT schemes (eg. Slater et al. 2001) and will be examined more as more research is done in this area.

f. Snow Liquid Water and Phase Change

The heat transfer is calculated from Eq. 1.8 assuming $F_{s\,i} = 0$. The phase change flux (W m^{-2}) is simply the sum of the available energy for snow melt ($F_{sm\,i}$) and liquid water freezing ($F_{sf\,i}$) where

$$\begin{aligned} F_{sm\,i} &= \min\left[c_{s\,i}\,D_{s\,i}\,\left(T_{s\,i} - T_f\right),\; L_f\left(W_{s\,i} - W_{l\,i}\right)\right]/\Delta t \\ F_{sf\,i} &= \min\left[c_{s\,i}\,D_{s\,i}\,\left(T_f - T_{s\,i}\right),\; L_f W_{l\,i}\right]/\Delta t \;\; . \\ F_{s\,i} &= F_{sm\,i} - F_{sf\,i} \end{aligned}$$

The snow temperature and liquid water content (see below) are then updated.

The liquid water content of the snow is modeled as a series of bucket-type reservoirs. Local changes during a model time step arise due to snow melt, water freezing, evaporation and liquid flow so that

$$\frac{\partial W_{l\,i}}{\partial t} = R_{l\,i-1} - R_{l\,i} + F_{s\,i}/L_f \qquad\qquad (W_{l\,i} \le W_{l\,i\,\max}) \;\; , \qquad (1.18)$$

where R_l represents the water flow between layers (kg m^{-2} s^{-1}), and the flux at the snow surface is

$$R_{l\,0} = P_{rn} - (1 - \chi_1)\; E_n \;\; .$$

Each snow layer has a maximum liquid water holding capacity which is expressed following Anderson (1976) as

$$W_{l\,i\,\max} = W_{s\,i}\,\left[r_{W\,\min} + \left(r_{W\,\max} - r_{W\,\min}\right)\max\left(0,\,\rho_r - \rho_{s\,i}\right)/\rho_r\right] \;\; , \qquad (1.19)$$

where the constants $r_{W\,\max} = 0.10$, $r_{W\,\min} = 0.03$, and $\rho_r = 200$ kg m^{-3}. A liquid water flux is generated ($R_l > 0$) when the liquid water content exceeds this threshold:

$$R_{l\,i} = \max\left(0,\ W_{l\,i} - W_{l\,i\,\max}\right)/\Delta t \ , \tag{1.20}$$

The water flow could be governed by a relation describing the hydraulic conductivity of the snow (eg. Jordan 1991), but this does not seem to be currently warrented given the rather simple complexity of the three-layer scheme. In addition, CROCUS abandoned the aforementioned method in favor of the series-of-buckets method as it was found the two results gave nearly identical total daily runoff.

Snowmelt within a layer impacts the mass distribution in two ways. First, the snow layer thickness is compacted at a rate proportional to the amount of snow melt retained in the snow layer (Lynch-Stieglitz 1994), leading to densification:

$$D'_{s\,i} = D_{s\,i}\ \left[\frac{\min\left(W_{l\,i} + F_{sm\,i}\Delta t/L_f,\ W_{l\,i\,\max}\right)}{W_{l\,i}}\right] \tag{1.21}$$

$$\rho'_{s\,i} = D_{s\,i}\,\rho_{s\,i}/D'_{s\,i} \tag{1.22}$$

so that the over mass or SWE is unchanged. Second, any melt water in excess of the layer holding capacity leaves the snow layer which is modelled as a decrease in thickness:

$$D'_{s\,i} = D_{s\,i} - \frac{1}{\rho_{s\,i}}\left[\max\left(\frac{F_{sm\,i}\Delta t}{L_f} + W_{l\,i} - W_{l\,i\,\max},\ 0\right)\right] \ , \tag{1.23}$$

resulting in a loss of mass from this layer (as the layer-average density is unchanged). It is also possible for both processes [Eq.s (1.21)-(1.23)] to occur during a single time step. It can be seen from Eq. (1.23) that if the layer i is saturated, then the total loss in mass is proportional to $F_{sm\,i}$. Note that a mass loss following Eq. (1.23) generates liquid water outflow from layer i [Eq. (1.20)].

The water flow solution procedure starts from the uppermost layer and proceeds downward. Water entering a layer refreezes if their is sufficient cold content. Once a layer can no longer freeze existing water (i.e. $T_{s\,i} = T_f$), then the unfrozen water is retained up to the maxmum holding capacity. The refreezing and water retention processes increase the layer-average density and mass. Water flow processes do not impact the layer thicknesses. Water leaving the lowest snow layer ($R_{l\,N}$) is available for partitioning into soil water infiltration and surface runoff by the SVAT scheme.

2. Coupling to ISBA

An important aspect of coupling with the land surface is the parameterization of the FSCA, as it is used to partition the fluxes of heat, momentum and mass between the snow and non-snow covered fractions of the grid box. The FSCA is defined as

$$p_{ng} = \left[W_s / \left(a_{pn}\, W_s + W_{np}\right)\right]^{b_{pn}} \qquad (0 \le p_{ng} \le 1) \tag{1.24}$$

$$p_{nc} = \left[D_s / \left(D_s + c_{pn}\, z_0\right)\right]^{b_{pn}} \qquad (0 \le p_{nc} < 1) \tag{1.25}$$

$$p_n = (1 - veg)\, p_{ng} \; + \; veg\, p_{nc} \tag{1.26}$$

where p_n represents the total grid box FSCA. The soil and canopy or vegetation FSCA are represented by p_{ng} and p_{nc}, respectively. The soil/vegetation surface roughness length is z_0. The parameters a_{pn}, b_{pn}, c_{pn} and W_{np} can be adjusted depending on the modeled spatial scale and the associated degree of sub-grid heteorgeneity (i.e. the effects of trees and snow patchiness caused by relief).

These relationships for FSCA are fairly standard among SVATs used for atmospheric model applications (eg.s Pitman et al. 1991; Verseghy 1991; Yang et al. 1997), however the values of the coefficients vary among the schemes. In ISBA, the parameter a_{pn} is equal to 0 for cases with relatively flat bare ground or short vegetation cover, otherwise it is equal to one (which is usually the case for relatively

large scales). The value for b_{pn} is usually unity in ISBA, but it can be reduced for large scales for which sub-grid patchiness of snow is enhanced (Brun et al. 1997). The parameter c_{pn} is related to the vegetation characteristics. The ISBA-ES default value of W_{np} is W_{crn} (Douville et al. 1995).

The ISBA-ES soil-vegetation surface energy budget equation is written using a similar expression to that used by CROCUS (coupled to ISBA; Etchevers 2000) as

$$\begin{aligned}\frac{1}{C_T}\frac{\partial T_s}{\partial t} = &(1-p_n)\left[R_g\,(1-\alpha)+\epsilon\left(R_{at}-\sigma {T_s}^4\right)-H-LE\right] \\ &+\ p_n\ \left[J_{s\,N}+Q_{s\,N}+c_w\,R_{l\,N}\ (T_f-T_s)\right] \\ &-\ \frac{2\pi}{\tau C_T}\,(T_s-T_2)+L_f\,F_{sw} \end{aligned} \tag{1.27}$$

where the sub-surface restore temperature is given by T_2 and the surface soil-vegetation temperature is represented by T_s. The last term on the right hand side of Eq. 1.27 represents latent heat release or absorbtion due to phase changes of soil moisture between ice and liquid (Boone et al. 2000). Note that this definition of T_s is different from that used by ISBA-FR which includes the upper layer of the snowpack and therefore includes the snow thermal properties in the definition of C_T (as opposed to CROCUS and ISBA-ES) along with the thermal properties of the soil/vegetation. The albedo and emissivity for the snow-free portion of the grid box are represented by α and ϵ, respectively.

The fluxes between the atmosphere and the snow/vegetation are weighted by $1-p_n$, while the fluxes at the base of the snowpack are weighted by p_n. The term involving the snow runoff ($R_{l\,N}$) in Eq. (1.27) represents an advective term. This rather simple snow/surface coupling was found to produce reasonable sub-surface soil temperatures, soil/snow heat fluxes, infiltration and runoff for CROCUS for an alpine site (Etchevers 2000) and a cold continental climate (Schlosser et al. 2000; Slater et al. 2001). Note that an option to use a multi-layer explicit soil model

underlying the snow (soil temperature is modeled using diffusion, water flow is modeled using Richard's equation and soil ice is considered in each layer) is also available (for details see Boone et al. 2000 and Boone 2000).

The snow cover is discerned from the soil-vegetation layer in ISBA-ES (Etchevers 2000) so that the soil-snow heat flux is explicitly modeled. It is written with the aid of Eq. (1.11) as

$$J_{s\,N} = 2\left(D_{s\,N}\Lambda_{s\,N} + \Delta z_1 \lambda_s\right) \frac{\left(T_{s\,N} - T_s\right)}{\left(D_{s\,N} + \Delta z_1\right)^2} \ . \tag{1.28}$$

The soil thermal conductivity (λ_s) is estimated following Etchevers (2000) using the relationships for thermal conductivity from Noilhan and Planton (1989). The upper layer soil thickness (Δz_1) is several centimeters thick.

The area-averaged atmospheric fluxes from a grid box are calculated as the sum of the surface fluxes from the snow weighted by p_n and the fluxes from the soil/vegetation weighted by $(1 - p_n)$. The shortwave radiation absorbed by the soil surface at the base of the snow cover is given as

$$Q_{s\,N} = R_g\left(1 - \alpha\right)\left(1 - \alpha_n\right)\exp\left(-\nu_{s\,N}\, z_N\right)$$

where one reflection (from the underlying soil/vegetation cover) is accounted for, and α is the albedo of the underlying soil/vegetation surface. Precipitation in the form of snow falls only the snow covered portion of the grid box, whereas liquid precipitation is paritioned between the snow-covered and snow-free portions of the surface using the snow fraction. The multi-layer snow model is activated if snow falls or there is snow on the surface. The solution procedure for ISBA-ES is outlined in Appendix C.

APPENDIX A

SYMBOLS

C_H	-	turbulent exchange coefficient
C_T	m^2 K J^{-1}	surface soil/vegetation thermal inertia
C_p	J kg^{-1} K^{-1}	specific heat of air
C_ν	$m^{5/2}$ kg^{-1}	radiation extinction coefficient parameter
$D_{s\,i}$	m	snow layer thickness
$D_{s\,1\,\max}$	m	maximum uppermost snow layer thickness
E_n	kg m^{-2} s^{-1}	sublimation/evaporation rate from snow surface
$F_{s\,i}$	W m^{-2}	snow total phase change term
$F_{sf\,i}$	W m^{-2}	snow phase (freeze) change term
$F_{sm\,i}$	W m^{-2}	snow phase (melt) change term
F_{sw}	W m^{-2}	surface soil ice/water phase change term
$\mathcal{F}$	W m^{-2}	fluxes
$G_{s\,i}$	W m^{-2}	total snow heat fluxes
H	W m^{-2}	sensible heat flux from snow-free area
H_n	W m^{-2}	sensible heat flux from snow surface
$H_{s\,i}$	J m^{-2}	snow layer heat content
$\overline{H}_s$	J m^{-2}	total snow heat content
H^*	W m^{-2}	total surface sensible heat flux
$J_{s\,i}$	W m^{-2}	conduction heat flux (diffusion)
LE	W m^{-2}	latent heat flux from snow-free area
LE_n	W m^{-2}	latent heat flux from snow surface
LE^*	W m^{-2}	total surface latent heat flux
L_f, L_s, L_v	J kg^{-1}	latent heats of fusion, sublimation and vaporization
N_s	-	number of snow model layers
P_n	kg m^{-2} s^{-1}	snowfall rate
P_r	kg m^{-2} s^{-1}	total rain rate
P_{rn}	kg m^{-2} s^{-1}	rain rate over snowpack
$Q_{s\,i}$	W m^{-2}	solar radiation transmission term

R_{at}	W m^{-2}	downwelling longwave atmospheric radiation
R_g	W m^{-2}	solar radiation (diffuse and direct)
R_i	-	Richardson number
$R_{i\,\max}$	-	maximum or critical Richarson number
R_n	W m^{-2}	net radiation flux
$R_{l\,i}$	kg m^{-2} s^{-1}	snowpack liquid water flow rate
$R_{l\,N_s}$	kg m^{-2} s^{-1}	snowpack liquid water runoff or total outflow rate
R_n^*	W m^{-2}	total surface net radiation
T_a	K	air temperature
$T_{a\,l}$	K	temperature of liquid precipitation
T_f	K	triple point temperature for water
T_s	K	composite soil/vegetation surface temperature
$T_{s\,i}$	K	average snow layer temperature
T_2	K	soil/vegetation restore temperature
V_a	m s^{-1}	wind speed
W_{crn}	kg m^{-2}	critical SWE
$W_{l\,i}$	kg m^{-2}	snow layer liquid water content
W_{np}	kg m^{-2}	generalized critical SWE
$W_{l\,i\,\max}$	kg m^{-2}	maximum snow layer liquid water content
$W_{s\,i}$	kg m^{-2}	snow layer SWE
Z_a, Z_b, Z_c	s^{-1}	surface energy budget linearization terms
a_i, b_i, c_i	W m^{-2} K^{-1}	snow temperature matrix coefficients
a_{pn}, b_{pn}, c_{pn}	-	snow fraction parameters
a_{sc}	s^{-1}	snow settling parameter
b_{sc}	K^{-1}	snow settling parameter
c_{sc}	m^3 kg^{-1}	snow settling parameter
a_{sd}	m	snow grain size parameter
b_{sd}	m^{13} kg^{-4}	snow grain size parameter
a_{sn}	kg m^{-3}	snowfall density parameter
b_{sn}	kg m^{-3} K^{-1}	snowfall density parameter
c_{sn}	kg s$^{-1/2}$ m$^{-7/2}$	snowfall density parameter
a_η	K^{-1}	snow viscocity parameter
b_η	m^{-3} kg^{-1}	snow viscocity parameter
a_λ	W m^{-1}	snow thermal conductivity parameter
b_λ	W m^5 K^{-1} kg^{-1}	snow thermal conductivity parameter

$a_{\lambda v}$	W m^{-1} K^{-1}	snow thermal conductivity (vapor) parameter
$b_{\lambda v}$	W m^{-1}	snow thermal conductivity (vapor) parameter
$c_{\lambda v}$	K	snow thermal conductivity (vapor) parameter
c_I	J kg^{-1} K^{-1}	specific heat of ice
c_i	J K^{-1} m^{-3}	heat capacity of ice
$c_{s\,i}$	J K^{-1} m^{-3}	snow layer heat capacity
c_w	J kg^{-1} K^{-1}	specific heat of liquid water
$d_{s\,i}$	m	snow grain size
f_i	W m^{-2} K^{-1}	snow temperature matrix forcing function
i	-	snow vertical index
k	-	von Karman constant
p	Pa	surface pressure
p_n	-	total snow fraction
p_{nc}	-	vegetation snow cover fraction
p_{ng}	-	bare-soil snow cover fraction
p_0	Pa	reference atmospheric pressure
q_a	kg kg^{-1}	atmospheric specific humidity
$q_{\rm sat}$	kg kg^{-1}	surface specific humidity
$r_{w\,\max}$	-	maximum snow liquid water content parameter
$r_{w\,\min}$	-	maximum snow liquid water content parameter
veg	-	surface vegetation cover fraction
z_a	m	height of air temperature forcing
$z_{s\,i}$	m	depth in snowpack from atmosphere/snow interface
z_u	m	height of wind forcing
z_{0t}	m	effective surface roughness length
Δt	s	model time step
Δz_1	m	thickness of surface soil layer
$\Lambda_{s\,i}$	W m^{-1} K^{-1}	effective snow layer thermal conductivity
$\overline{\Lambda}_{s\,i}$	W m^{-1} K^{-1}	interfacial effective snow layer thermal conductivity
α	-	soil/vegetation albedo
α_n	-	snow albedo
α_{nd}	-	albedo of dry snow
α_{nw}	-	albedo of wet snow
$\alpha_{n\,\rm new}$	-	albedo of freshly fallen snow
$\alpha_{\max}$	-	maximum snow albedo

$\alpha_{\min}$	-	minimum snow albedo
χ_i	-	snow layer frozen fraction
χ_s	-	weight for effective temperature at snowpack base
δ_D	-	delta function for snow grid
δ_s	-	delta function for snow mass and heat redistribution
ϵ	-	soil/vegegtation surface emissivity
ϵ_n	-	snow surface emissivity
$\eta_{s\,i}$	Pa s^{-1}	snow viscocity
η_0	Pa s^{-1}	snow viscocity coefficient
$\lambda_{s\,i}$	W m^{-1} K^{-1}	snow thermal conductivity
$\lambda_{sv\,i}$	W m^{-1} K^{-1}	snow thermal conductivity from vapor transfer
$\nu_{s\,i}$	m^{-1}	shortwave radiation extinction coefficient
ρ_a	kg m^{-3}	air density
ρ_i	kg m^{-3}	ice density
ρ_r	kg m^{-3}	maximum liquid water content parameter
ρ_{sc}	kg m^{-3}	snow settling parameter
$\rho_{s\,i}$	kg m^{-3}	average snow layer density
ρ_{new}	kg m^{-3}	density of snowfall
ϱ_i	W m^{-2} K^{-1}	snow temperature solution coefficient
σ	W m^{-2} K^{-4}	Stefan-Botzmann constant
$\sigma_{s\,i}$	Pa	pressure of the overlying snow
τ	s	time constant (one day)
τ_a	s	albedo time constant for dry snow
τ_f	s	albedo time constant for wet snow
ω_α	-	degree of snow saturation

APPENDIX B

PARAMETERIZATION SCHEMES FOR ISBA-ES

1. Snow viscosity

The snow viscosity is formulated as a function of snow density (Kojima 1967) and temperature (Mellor 1964) as

$$\eta_{s\,i} = \eta_0 \exp\left[a_\eta \left(T_f - T_{s\,i}\right) + b_\eta \rho_{s\,i}\right] \quad , \tag{B.1}$$

where $\eta_0 = 3.7 \times 10^7$ Pa s, $a_\eta = 8.1 \times 10^{-2}$ K^{-1} and $b_\eta = 1.8 \times 10^{-2}$ m^3 kg^{-1}. An example of snow compaction for the three layer model is shown in Fig. B.1. The sensitivity to snow temperature (which enters into the compaction calculation via the viscosity coefficient in Eq. B.1) for two arbitrary values is shown. Snow settling is the dominant compaction mechanism initially (see Eq. 1.6) for low density snow, whereas compaction due to overburden is the primary mechanism over longer time periods and for higher density snow.

2. Snowfall density

The snowfall density is expressed using the expression from CROCUS as

$$\rho_{\rm new} = a_{sn} + b_{sn}\left(T_a - T_f\right) + c_{sn}\left(V_a\right)^{1/2} \qquad \left(\rho_{\rm min} \geq 50 \text{ kg m}^{-3}\right) \quad , \tag{B.2}$$

where T_a represents the air temperature (K), and V_a is the wind speed (m s^{-1}). The coefficients $a_{sn} = 109$ kg m^{-3}, $b_{sn} = 6$ kg m^{-3} K^{-1}, and $c_{sn} = 26$ kg m$^{-7/2}$ s$^{1/2}$. The dependence on wind speed results as relatively high winds can break down the falling flakes into finer grains. Snowfall density as a function of temperature and wind speed is shown in Fig. B.2.

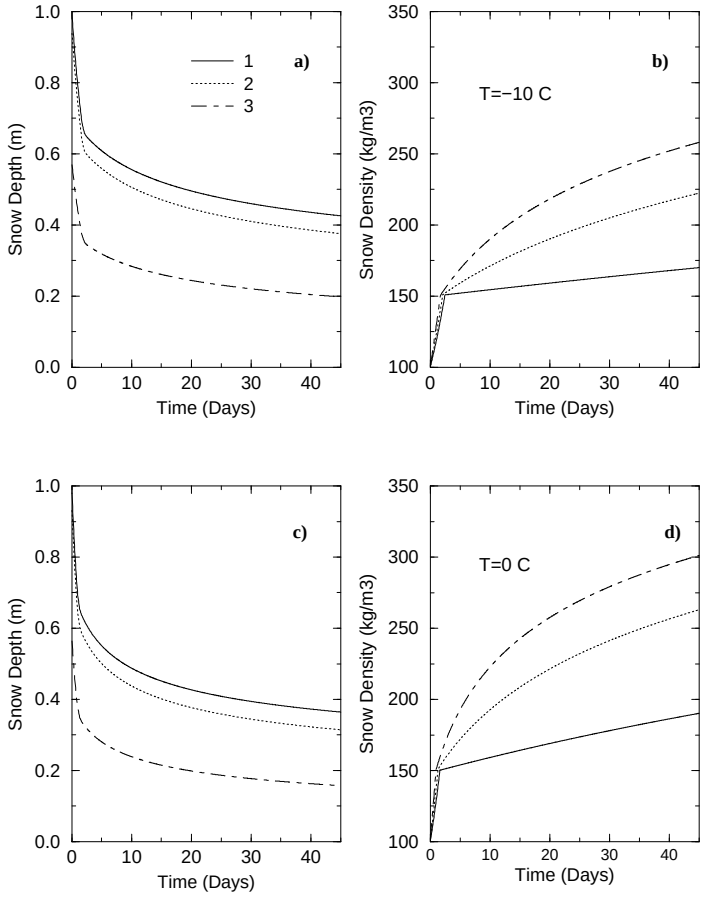

FIG. B.1. Snow compaction for a 1 m snowpack with constant temperature and initial constant density profiles. The snow depths are shown in the left panels, and the corresponding snow densities are shown on the right for three snow layers. The upper panel tests use a constant snow temperature of -10 C, while the lower panel tests use 0 C.

3. Thermal Properties

The snow heat capacity is defined following Verseghy (1991) as

$$c_{s\,j} = c_i\,\rho_{s\,i}/\rho_i = c_I\,\rho_{s\,i} \tag{B.3}$$

where c_i is the heat capacity of ice (J K^{-1} m^{-3}), c_I is the specific heat of ice (2047 J K^{-1} kg^{-1}), and the ice density is $\rho_i = 920$ kg m^{-3}.

The effective thermal conductivity is defined as

$$\Lambda_{s\,i} = \lambda_{s\,i} + \lambda_{sv\,i} \tag{B.4}$$

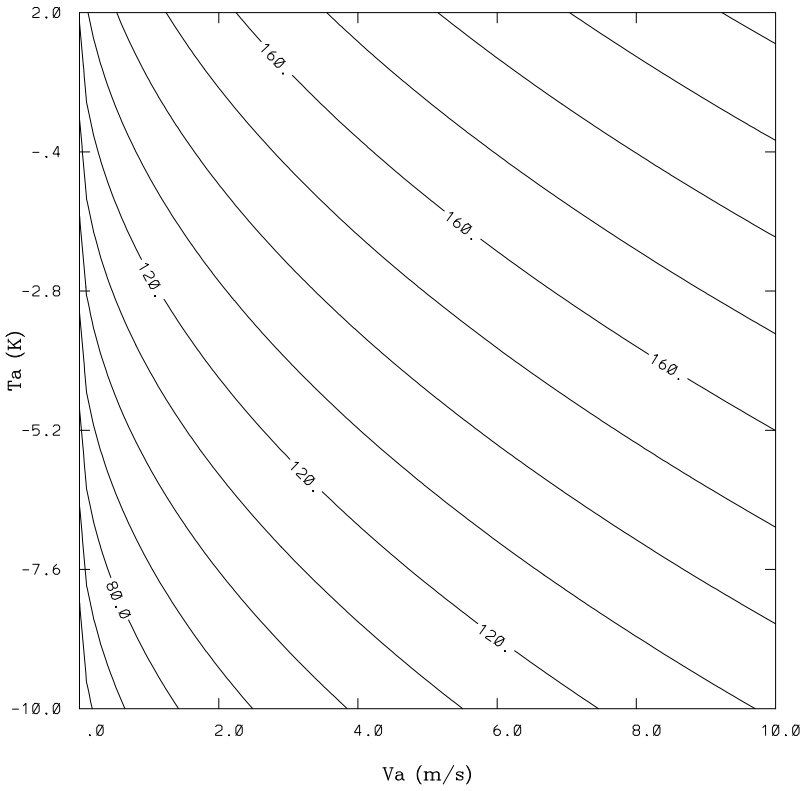

FIG. B.2. The density of snow falling on the surface as a function of air temperature (T_a) and wind speed (V_a) from Eq. B.2.

$$\lambda_{s\,i} = a_\lambda + b_\lambda \rho_{s\,i}^2 \tag{B.5}$$

$$\lambda_{sv\,i} = \left(a_{\lambda v} + \frac{b_{\lambda v}}{T_{s\,i} + c_{\lambda v}} \right) \left(\frac{p_0}{p} \right) \tag{B.6}$$

where Eq. B.5 corresponds to the snow thermal conductivity, and $a_\lambda = 0.02$ W m^{-1} K^{-1} and $b_\lambda = 2.5 \times 10^{-6}$ W m^5 K^{-1} kg^{-2} (Anderson 1976). Eq. B.6 represents the thermal conductivity from vapor transfer in the snow (Sun et al. 1999), where p is the atmospheric pressure in hPa, and $p_0 = 1000$ hPa. The coefficients were determined by Sun et al. (1999) to provide results which best approximated the physically based and more complicated equation of Jordan (1991): $a_{\lambda v} = -0.06023$

W m^{-1} K^{-1}, $b_{\lambda v} = -2.5425$ W m^{-1}, and $c_{\lambda v} = -289.99$ K. The λ_{sv} contribution to the effective thermal conductivity can be significant for fresh snow (i.e. relatively low snow densities), high altitudes and warm temperatures. A comparison of λ_s and λ_{sv} for various pressures and temperatures are shown in panels g-i of Fig. B.3.

4. Shortwave radiation absorption

In Eq. 1.10, ν_s is the extinction coefficient for shortwave radiation (m^{-1}) which is written following Bohren and Barkstrom (1974) as

$$\nu_{s\,i} = C_\nu \, \rho_{s\,i} \, {d_{s\,i}}^{-1/2} \ , \tag{B.7}$$

where $C_\nu = 3.8 \times 10^{-3}$ m$^{5/2}$ kg^{-1}. the extinction coefficient is shown as a function of snow density in Fig. B.3e. The expression for snow grain size d_s is from Anderson (1976):

$$d_{s\,i} = a_{sd} \ + \ b_{sd} \, \rho_{s\,i}^4 \ , \tag{B.8}$$

where $a_{sd} = 1.6 \times 10^{-4}$ m and $b_{sd} = 1.1 \times 10^{-13}$ m^{13} kg^{-4}. The snow grain size is shown as a function of snow density in Fig. B.3b. Note that in contrast to the aforementioned figure, the snow grain size is limited at 2.796 $\times 10^{-3}$ m. An example of the shortwave radiation extinction within the snowpack is shown in Fig. B.3d as a function of snow depth for three constant snow density vertical distributions.

5. Snow albedo

The snow albedo is modeled using the same decrease and increase rate formulations as Douville et al. (1995). A linear decrease rate is used for dry snow (from Baker et al. 1990) and an exponential decrease rate is used to model the wet metamorphism (from Verseghy 1991). The snow albedo increases at a rate proportional to the snowfall. The relationships describing the albedo rates of change during a

time step are

$$\alpha_{nd}^{n} = \alpha_{n}^{n-1} \; - \; \tau_a \Delta t / \tau \tag{B.9}$$

$$\alpha_{nw}^{n} = \left(\alpha_{n}^{n-1} \; - \; \alpha_{\min}\right) \exp\left(-\tau_f \Delta t / \tau\right) \; + \; \alpha_{\min} \tag{B.10}$$

$$\alpha_{n\,\mathrm{new}} = \left[P_n \Delta t / \left(\rho_w \, W_{crn}\right)\right] \left(\alpha_{\max} - \alpha_{\min}\right) \quad , \tag{B.11}$$

where α_{nd} corresponds to dry snow and α_{nw} is used for wet (melting) snow. The following values from Douville et al. (1995) are used for the model parameters: the time constants $\tau_a = 0.008$ s, $\tau_f = 0.24$ s and $\tau = 86400$ s, the minimum snow albedo is $\alpha_{\min} = 0.50$, and the maximum albedo $\alpha_{\max}$ is assigned a value of 0.85.

The updated snow albedo is expressed in the current study as

$$\alpha_{n}^{n} = \left(1 - \omega_\alpha\right) \, \alpha_{nd}^{n} \; + \; \omega_\alpha \, \alpha_{nw}^{n} \; + \; \alpha_{\mathrm{new}} \qquad\qquad \left(\alpha_{\min} \leq \alpha_n \leq \alpha_{\max}\right) \tag{B.12}$$

The weight ω_α is defined as the degree of saturation when snow is melting, otherwise it is zero:

$$\begin{aligned} \omega_\alpha &= 1 - \chi_1 \qquad\qquad && \left(F_{s\,1} > 0\right) \\ \omega_\alpha &= 0 \qquad\qquad && \left(F_{s\,1} \leq 0\right) \end{aligned} \tag{B.13}$$

so that the snow albedo decreases more rapidly when the degree of snow saturation with respect to liquid water is larger. The decay of snow albedo as a function of time is shown in Fig. B.3a for four different (constant) degrees of snow liquid saturation.

It is planned that the albedo parameterization will eventually be replaced by a method which incorporates the uppermost layer density or grain size and possibly a litter-deposition algorithm: but the relatively simple method outlined here will be retained until such a scheme has been incorporated.

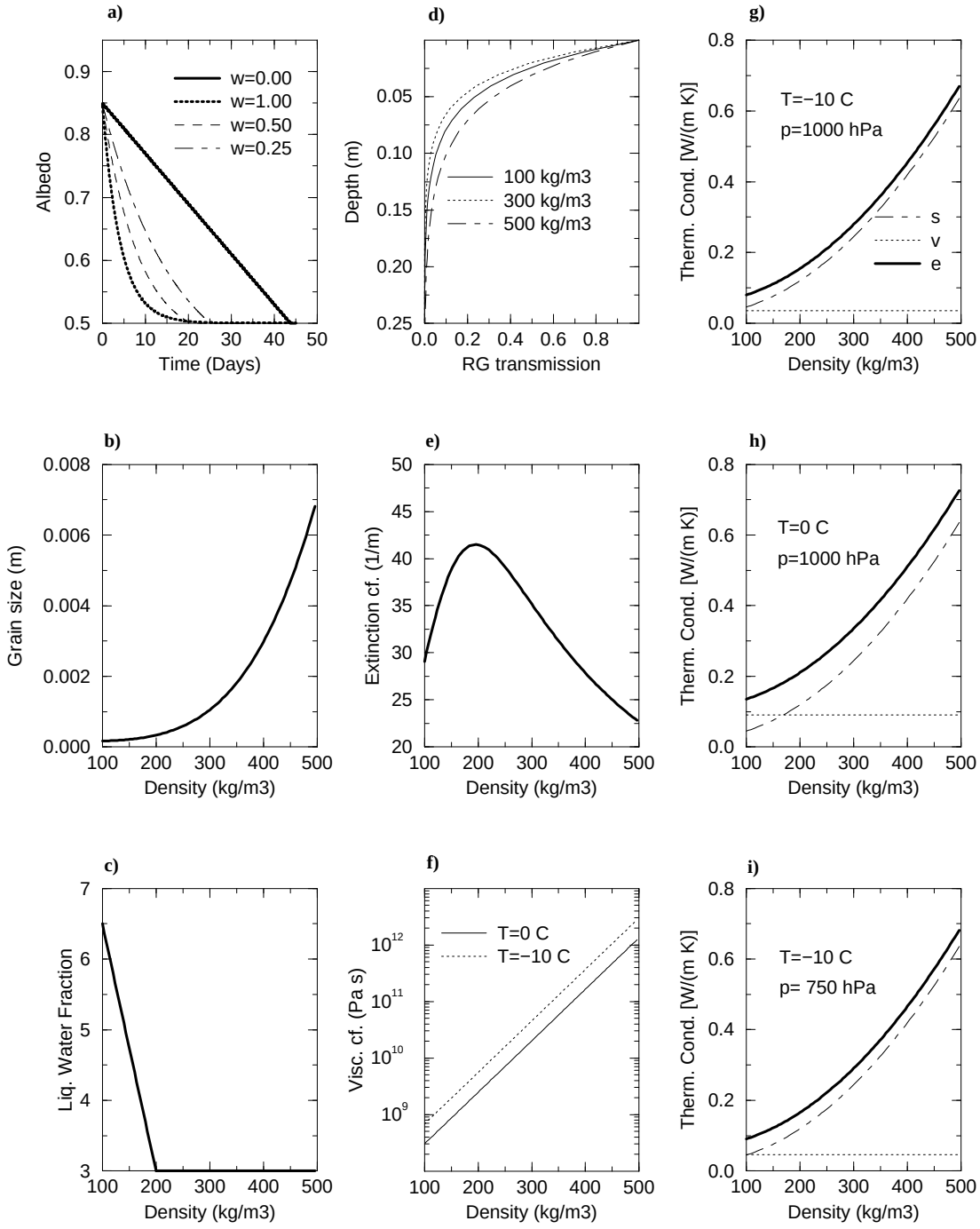

FIG. B.3. Snow physical parameterization schemes and coefficients: Panel a) snow albedo for varying degrees of liquid water saturation, w (equivalent to ω_α in Eq. B.13), b) grain size (d_s,Eq. B.8), c) maximum liquid water fraction in % (see Eq. 1.19), d) R_G transmission within the snowpack (see Eq. 1.10), e) radiation extinction coefficient (ν_s, Eq. B.7), f) viscosity coefficient (η_s, Eq. B.1), and g)-i) snow (λ_s: dashed line), vapor (λ_v: dotted line) and effective or total (Λ_s: solid line) thermal conductivities for various values of temperature and pressure (Eq. B.4).

6. Snow heat and mass redistribution

The model grid (D_i) is reset during each time step to the grid configuration defined from Eq.s (1.3)–(1.5). Note that the total snow depth is constant:

$$\sum_{i=1}^{N_s} D'_{s\,i} \;= \sum_{i=1}^{N_s} D_{s\,i} \tag{B.14}$$

While the mass and heat content of the entire snowpack are conserved during this transformation, the vertical distribution of snow mass and heat must be adjusted. Using the superscript $\prime$ to denote values after the grid transformation, the conservation equations for mass (or equivalently SWE) and heat are, respectively:

$$\sum_{i=1}^{N_s} W'_{s\,i} \;=\; \sum_{i=1}^{N_s} W_{s\,i} \qquad \text{and} \qquad \sum_{i=1}^{N_s} H'_{s\,i} \;=\; \sum_{i=1}^{N_s} H_{s\,i} \;, \tag{B.15}$$

The transformed SWE for layer j is updated from

$$W'_{s\,i} \;=\; W_{s\,i} + \Delta W_{s\,i} \;,$$

which is expressed for the uppermost and lowest layers as a function of snow density and thickness as

$$\rho'_{s\,1}\, D'_1 \;= \rho_{s\,1}\, D_1 \;+\; \Delta D_1 \left[\delta_{s\,1}\, \rho_{s\,2} + (1 - \delta_{s\,1})\; \rho_{s\,1}\right] \tag{B.16}$$

$$\begin{aligned} \rho'_{s\,N_s}\, D'_{N_s} \;&= \rho_{s\,N_s}\, D_{N_s} \;-\; \Delta D_{N_s-1} \\ &\qquad \left[\delta_{s\,N_s-1}\, \rho_{s\,N_s} + (1 - \delta_{s\,N_s-1})\; \rho_{s\,N_s-1}\right] \end{aligned} \tag{B.17}$$

respectively. The grid thickness change ($\Delta D_i \;=\; z'_i \;-\; z_i$) results from the grid resetting. The depth in the snowpack (z_i) is the vertical coordinate, such that $z_0 = 0$ at the atmosphere-snow interface, and z_i increases downward towards the soil such that $z_N = D_s$. The function $\delta_{s\,i}$ is defined as

$$\delta_{s\,i} \;= \begin{cases} 0 & \Delta D_i \le 0 \\ \\ 1 & \Delta D_i > 0 \end{cases} \quad .$$

From Eq.s B.16 and B.17, if layer 1 or N_s decrease in thickness, the density remains unchanged (i.e. $\rho'_{s\,i} = \rho_{s\,i}$) and mass (or SWE) reduction is accomplished by reducing the layer thickness. If the layer thickness increases, then density is also updated. The equation for the intermediate layers is defined using Eq.s B.16 and B.17 as

$$\begin{aligned}\rho'_{s\,i}\,D'_i \;&= \rho_{s\,i}\,D_i \;-\; \Delta D_{i-1}\left[\delta_{s\,i-1}\,\rho_{s\,i} + (1-\delta_{s\,i-1})\;\rho_{s\,i-1}\right] \\ &\quad +\; \Delta D_i\left[\delta_{s\,i}\,\rho_{s\,i+1} + (1-\delta_{s\,i})\;\rho_{s\,i}\right] \qquad (i = 2, N_s - 1) \end{aligned} \tag{B.18}$$

A similar expression is used for the snow heat content in the uppermost and lowest layers, respectively:

$$\begin{aligned} H'_{s\,1} \;&=\; H_{s\,1} \;+\; \Delta D_1\left[\delta_{s\,1}\,\frac{H_{s\,2}}{D_2} + (1-\delta_{s\,1})\;\frac{H_{s\,1}}{D_1}\right] \\ H'_{s\,N_s} \;&=\; H_{s\,N_s} \;-\; \Delta D_{N_s-1}\left[\delta_{s\,N_s-1}\,\frac{H_{s\,N_s}}{D_{N_s}} + (1-\delta_{s\,N_s-1})\;\frac{H_{s\,N_s-1}}{D_{N_s-1}}\right] \end{aligned}$$

and for the intermediate layers:

$$\begin{aligned} H'_{s\,i} \;&= H_{s\,i} \;-\; \Delta D_{i-1}\left[\delta_{s\,i-1}\,\frac{H_{s\,i}}{D_i} + (1-\delta_{s\,i-1})\;\frac{H_{s\,i-1}}{D_{i-1}}\right] \\ &\quad +\; \Delta D_i\left[\delta_{s\,i}\,\frac{H_{s\,i+1}}{D_{i+1}} + (1-\delta_{s\,i})\;\frac{H_{s\,i}}{D_i}\right] \end{aligned} \tag{B.19}$$

The transformed heat content ($H'_{s\,i}$) is used to update the liquid water content and the temperature of the snow layer. The transformed snow density is updated using Eq.s B.16 and B.17 as the thickness change is known.

APPENDIX C

SOLUTION PROCEDURE FOR ISBA-ES

The basic solution procedure for ISBA-ES each time step is described below.

i) At the beginning of the time step, the snow fraction is calculated [Eq.s (1.24)-(1.26)].

ii) Snowfall mass and heat content are added to the uppermost snow layer. $\rho_{s\,1}$, $D_{s\,1}$, $T_{s\,1}$ and $W_{l\,1}$ are updated accordingly. Snowfall is assumed to have the same temperature as the uppermost snow layer upon reaching the surface, therefore the advective heat flux from snowfall can be neglected (in the surface energy budget).

iii) The snow thicknesses are reset [Eq.s (1.3)-(1.4)] and the vertical profiles of mass and heat are redistributed while conserving the total snow pack mass and heat [Eq. (B.15)].

iv) $H_{s\,i}$, $\rho_{s\,i}$ and $D_{s\,i}$ are used to diagnose $T_{s\,i}$ and $W_{l\,i}$ [Eq. (1.7)].

v) Settling is calculated [Eq. (1.6)] and $\rho_{s\,i}$ and $D_{s\,i}$ are updated. Snow mass and heat content are unaltered.

vi) Shortwave radiation transmission ($Q_{s\,i}$) [Eq. (1.10)] and surface snow albedo (α_n) [Eq. (B.12)] are calculated along with the snow thermal conductivity ($\Lambda_{s\,i}$).

vii) The linearized system of equations is solved simultaneously [Eq. (1.8)] to estimate the preliminary profile of $T_{s\,i}$ and the surface fluxes ($G_{s\,0}$) [Eq. (1.14)].

viii) If melting occurs, the surface energy budget and fluxes are re-calculated assuming an updated uppermost snow layer temperature at the freezing point (T_f). The lower two snow layer temperatures are also recalculated assuming $T_{s\,1} = T_f$.

ix) Phase changes ($F_{s\,i}$), water flow ($R_{l\,i}$) and changes in liquid water storage [Eq. (1.18)] are evaluated. Profiles of $T_{s\,i}$, $W_{l\,i}$, $\rho_{s\,i}$ and $D_{s\,i}$ are updated.

x) The heat content ($H_{s\,i}$) is updated from the profiles of $T_{s\,i}$, $W_{l\,i}$, $\rho_{s\,i}$ and $D_{s\,i}$, [Eq. (1.7)] and saved for the next time step along with the updated snow albedo and the profiles of $\rho_{s\,i}$ and $D_{s\,i}$. Snow surface fluxes (Eq. 1.14), runoff ($R_{l\,N}$) and the heat flux at the snow/soil/vegetation interface are output.

APPENDIX D

NUMERICAL METHODS

1. Surface Energy Budget

The surface energy budget for the snowpack surface is expressed using an implicit time integration scheme as

$$\frac{D_{s\,1}\, c_{s\,1}}{\Delta t}\left({T_{s\,1}}' - T_{s\,1}\right) = {R_n}' - {H_n}' - {LE}' + P_{rn}\, c_w\left(T_{a\,l} - T_f\right) - J'_{s\,1} - Q_{s\,1} \quad \text{(D.1)}$$

where $'$ denotes the value at time $t + \Delta t$. The flux terms at time $t + \Delta t$ are defined using either a backward difference approximation as

$$\mathcal{F}' = \mathcal{F} + \left(\partial\mathcal{F}/\partial T_{s\,1}\right)\left({T_{s\,1}}' - T_{s\,1}\right)$$

where $\mathcal{F}$ represents the fluxes (LE and R_n), or using the flux evaluated explicitly at time $t + \Delta t$ (as is done for $J_{s\,1}$ and H_n). The fluxes are linearized using the same standard form as the snow-free ISBA fluxes (Giordani 1993):

$${R_n}' = R_g\left(1 - \alpha_n\right) + \epsilon\left[R_{at} - \sigma {T_{s\,1}}^3\left(4{T_{s\,1}}' - 3T_{s\,1}\right)\right] \quad \text{(D.2)}$$

$${H_n}' = \frac{\rho_a}{R_a} C_p\left({T_{s\,1}}' - T_a\right) \quad \text{(D.3)}$$

$${LE}' = \left[L_v\left(1 - \chi_1\right) + L_s\chi_1\right]\frac{\rho_a}{R_a}\left[q_{\rm sat}\left(T_{s\,1}\right) - q_a + \frac{\partial q_{\rm sat}}{\partial T_{s\,1}}\left({T_{s\,1}}' - T_{s\,1}\right)\right] \quad \text{(D.4)}$$

$$J'_{s\,1} = 2\overline{\Lambda}_{s\,1}\frac{\left({T_{s\,1}}' - {T_{s\,2}}'\right)}{D_{s\,1} + D_{s\,2}} \quad \text{(D.5)}$$

Eq. D.1 can then be expressed as

$$\left(Z_a\, c_{s\,1} D_{s\,1}\right)\, {T_{s\,1}}' - \left(\frac{2\overline{\Lambda}_{s\,1}}{D_{s\,1} + D_{s\,2}}\right)\, {T_{s\,2}}' = c_{s\,1} D_{s\,1}\, \left(T_{s\,1}\, Z_b + Z_c\right) \quad \text{(D.6)}$$

where the coefficients are defined using Eq.s D.1-D.5 as

$$
\begin{aligned}
Z_a &= \frac{1}{\Delta t} + \frac{1}{c_{s\,1} D_{s\,1}} \Bigg\{ \frac{2\overline{\Lambda}_{s\,1}}{(D_{s\,1} + D_{s\,2})} + 4\epsilon\sigma {T_{s\,1}}^3 + \frac{\rho_a}{R_a} C_p + \\
&\quad \frac{\rho_a}{R_a} \frac{\partial q_{\rm sat}}{\partial T_{s\,1}} \left[L_v \left(1 - \chi_1\right) + L_s \chi_1 \right] \Bigg\} \\
Z_b &= \frac{1}{\Delta t} + \frac{1}{c_{s\,1} D_{s\,1}} \Bigg\{ 3\epsilon\sigma {T_{s\,1}}^3 + \\
&\quad \frac{\rho_a}{R_a} \frac{\partial q_{\rm sat}}{\partial T_{s\,1}} \left[L_v \ \left(1 - \chi_1\right) + L_s \, \chi_1 \right] \Bigg\} \\
Z_c &= \frac{1}{c_{s\,1} D_{s\,1}} \Bigg\{ \epsilon R_{at} \ + \ R_g (1 - \alpha) \ + \ \frac{\rho_a}{R_a} \, C_p \, T_a \\
&\quad - \frac{\rho_a}{R_a} \left[L_v \ \left(1 - \chi_1\right) + L_s \, \chi_1 \right] \left[q_{\rm sat} \left(T_{s\,1}\right) - q_a \right] \\
&\quad + P_{rn} \, c_w \left(T_{a\,l} - T_f\right) - Q_{s\,1} \Bigg\}
\end{aligned}
$$

2. Numerical solution for the snow profile

Eq. (1.8) can be written as a system of linear equations which can be solved quickly and with little storage because the equations can be cast in tridiagonal form. As a first step in the solution procedure, we neglect the phase change term ($F_{s\,i}$). The profile is adjusted for phase changes after the profile is initially calculated. Using the backward difference time scheme Eq. (1.8) can be written as

$$
\varrho_i \left(T'_{s\,i} - T_{s\,i}\right) \ = \ \frac{2\overline{\Lambda}_{s\,i-1} \left(T'_{s\,i-1} - T'_{s\,i}\right)}{D_{s\,i-1} + D_{s\,i}} \ - \ \frac{2\overline{\Lambda}_{s\,i} \left(T'_{s\,i} - T'_{s\,i+1}\right)}{D_{s\,i} + D_{s\,i+1}} + Q_{s\,i-1} - Q_{s\,i} \ , \tag{D.7}
$$

where $\varrho_i \ = \ D_i \, c_{s\,i} / \Delta t$. Note that the heat capacity and thermal conductivity are held constant for this calculation: this is a reasonable approximation for the time steps considered for this model.

Rearranging to have all of the terms involving the temperature at the time step $t + \Delta t$ (or $\prime$) from Eq. (D.7) on the left hand side yields

$$
a_i \, {T_{s\,i-1}}' \ + \ b_i \, {T_{s\,i}}' \ + \ c_i \, {T_{s\,i+1}}' \ = \ f_i \ , \tag{D.8}
$$

where the coefficients are defined as

$$\begin{aligned} a_i &= -2\overline{\Lambda}_{s\,i-1}/\left(D_{s\,i-1}+D_{s\,i}\right) \\ b_i &= \varrho_i + 2\overline{\Lambda}_{s\,i-1}/\left(D_{s\,i-1}+D_{s\,i}\right) + 2\overline{\Lambda}_{s\,i}/\left(D_{s\,i}+D_{s\,i+1}\right) \\ c_i &= -2\overline{\Lambda}_{s\,i}/\left(D_{s\,i}+D_{s\,i+1}\right) \ . \end{aligned}$$

The forcing function f is defined as

$$f_i = \varrho_i T_{s\,i} + Q_{s\,i-1} - Q_{s\,i} \ .$$

a. Solution Method

Eq. (D.8) represents a system of linear equations in T' which can be written in matrix form as

$$\mathbf{A}\hat{T} = \hat{f} \ , \tag{D.9}$$

where $\hat{T}$ and $\hat{f}$ are vectors of length N_s, and $\mathbf{A}$ is the $N_s \times N_s$ coefficient matrix. The solution is given by

$$\hat{T} = \mathbf{A}^{-1}\hat{f} \ . \tag{D.10}$$

The coefficient matrix is tridiagonal and the non-zero elements are represented by a, b and c:

$$\mathbf{A} = \begin{pmatrix} b_1 & c_1 & 0 \\ a_i & b_i & c_i \\ 0 & a_{N_s} & b_{N_s} \end{pmatrix} \ . \tag{D.11}$$

b. Boundary Conditions

1) Lower Boundary

At the lower boundary,

$$\begin{aligned} a_{N_s} &= -2\overline{\Lambda}_{s\,N_s-1}/\left(D_{s\,N_s-1}+D_{s\,N_s}\right) \\ b_{N_s} &= \varrho_N + 2\overline{\Lambda}_{s\,N-1}/\left(D_{s\,N_s-1}+D_{s\,N_s}\right) + 2\overline{\Lambda}_{s\,N}/\left(D_{s\,N_s}+\Delta z_1\right) \\ c_{N_s} &= 0 \\ f_{N_s} &= \varrho_{N_s} {T_{N_s}}^n + T_s 2\overline{\Lambda}_{s\,N_s}/\left(D_{s\,N_s}+\Delta z_1\right) + Q_{s\,N_s-1} - Q_{s\,N_s} \ . \end{aligned}$$

Note that the above implies that the lower boundary flux is expressed using a semi-implicit approach as

$$J_{s\,N} = \frac{2\overline{\Lambda}_{s\,N}\left(T'_{s\,N_s} - T_s\right)}{\left(D_{s\,N_s} + \Delta z_1\right)} \quad .$$

The flux between the soil and snowpack is conserved since this flux is passed directly to the soil when the soil/vegetation temperature T_s is updated. This is done so that the two energy budgets and profiles can be solved separately. As the soil/snow interfacial flux tends to be small, this results in a reasonable approximation (especially considering the time steps used by the model).

2) Upper Boundary

The matrix coefficients and forcing function for the first row elements (uppermost or surface layer) are then simply defined from Eq. D.6 as

$$\begin{aligned} a_1 &= 0 \\ b_1 &= \left(Z_a\, c_{s\,1} D_{s\,1}\right) \\ c_1 &= 2\overline{\Lambda}_{s\,1} / \left(D_{s\,1} + D_{s\,2}\right) \\ f_1 &= c_{s\,1} D_{s\,1}\left(T_{s\,1}\, Z_b + Z_c\right) \quad . \end{aligned}$$

3) Phase Change

At the end of the time step, the temperature profile and liquid water content are updated by evaluating the phase changes within the snow (F_s). However, if there is snow melt in the uppermost layer for 2 or more consecutive time steps, a slightly different approach is used (outline below).

c. Case of surface snowmelt

As in the detailed snow model CROCUS (Brun et al. 1992), the surface energy balance is calculated using an explicit method if there is melting for 2 or more consecutive time steps. The solution is exact and stable (as the surface temperature

is constant at T_f). The surface fluxes are then evaluated at T_f and the snow temperature profile in the lower two layers is evaluated using $T_{s\,1} = T_f$ as an upper boundary condition.

The surface energy budget is calculated as in Eq. D.1 except that the flux terms can be defined as

$$R_n{}' = R_g\,(1-\alpha_n) + \epsilon\left(R_{at} - \sigma {T_f}^4\right) \tag{D.12}$$

$$H_n{}' = \frac{\rho_a}{R_a} C_p\,(T_f - T_a) \tag{D.13}$$

$$LE' = \left[L_v\,(1-\chi_1) + L_s\chi_1\right]\frac{\rho_a}{R_a}\left[q_{\rm sat}\,(T_f) - q_a\right] \tag{D.14}$$

$$J'_{s\,1} = 2\overline{\Lambda}_{s\,1}\frac{(T_f - T'_{s\,2})}{D_{s\,1} + D_{s\,2}} \tag{D.15}$$

The snow temperature profile in the lower two layers is then calculated as presented in the previous section except by solving two linear equations (as opposed to 3) using $T'_{s\,1} = T_f$ as an upper boundary condition so that the matrix coefficients and forcing vector for layer 2 become

$$\begin{aligned}
a_2 &= 0 \\
b_2 &= \varrho_2 + 2\overline{\Lambda}_{s\,1}/\left(D_{s\,1} + D_{s\,2}\right) + 2\overline{\Lambda}_{s\,2}/\left(D_{s\,2} + D_{s\,3}\right) \\
c_2 &= -2\overline{\Lambda}_{s\,2}/\left(D_{s\,2} + D_{s\,3}\right) \quad . \\
f_2 &= \varrho_2\,T_{s\,2} + 2\,T_f\,\overline{\Lambda}_{s\,1}/\left(D_{s\,1} + D_{s\,2}\right) + Q_{s\,1} - Q_{s\,2} \quad .
\end{aligned}$$

Then the system of equations for a 3-layer configuration becomes

$$b_2 T'_2 + c_2 T'_3 = f_2 \tag{D.16}$$

$$a_2 T'_2 + b_2 T'_3 = f_3 \tag{D.17}$$

so that the solution for T'_2 is

$$T'_2 = \frac{f_2 - (c_2 f_3/b_2)}{b_2 - (c_2 a_2/b_2)} \tag{D.18}$$

which can then be used to obtain T_3'. Phase change adjustments in the lower two layers are then calculated. The flux between the first and second snow layers is then passed to the surface energy budget equation in order to maintain energy conservation.

APPENDIX E

EFFECTIVE ROUGHNESS LENGTH

The snow cover is assumed to reduce the gridbox effective roughness length following the averaging method from Noilhan and Lacarrére (1995):

$$\frac{1}{\ln\left[z_r/z_{0t}\right]^2} = \frac{p_n}{\ln\left[z_r/z_{0n}\right]^2} + \frac{(1-p_n)}{\ln\left[z_r/z_0\right]^2} \ , \tag{E.1}$$

where z_0 is the vegetation/surface roughness length (m), z_{0n} is the snow surface roughness length baseline value (0.001 m), and z_r is the blending height. See Eq.s 1.24-1.26 for the snow fraction (FSCA) expressions. The FSCA for the vegetation and the bare soil are shown in Fig. E.1 as a function of snow depth assuming a constant mean snowpack density of 300 kg m^{-3} and for varying values of the vegetation/surface roughness length (where Pnv represents p_{nc} and Png represents p_{ng}).

The effective surface roughness length (z_{0t}) is shown for varying values of z_r and veg in Fig. E.2 for roughness lengths varying as in Fig. E.1. Note that the effective roughness length decreases most rapidly with increasing snow depth as the vegetation cover fraction decreases. For relatively tall vegetation (large values of veg and z_0), the effective surface roughness changes the least owing to snow cover. The influence of the snow on the roughness length for relatively low ground cover is much more pronounced.

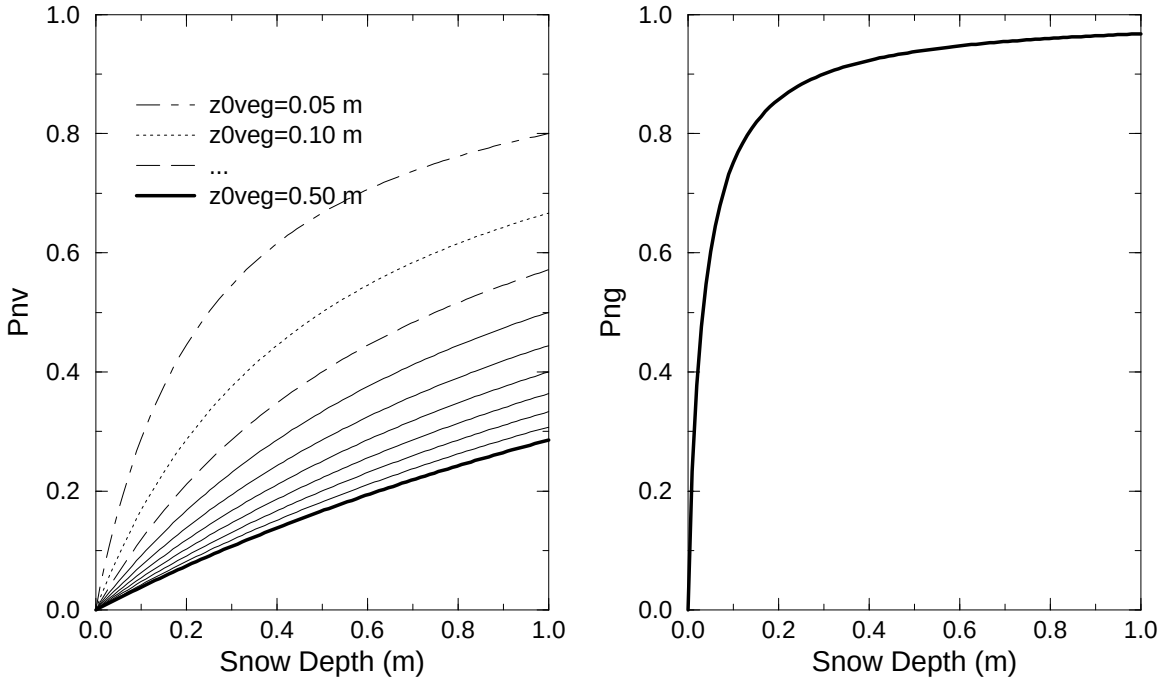

FIG. E.1. Snow cover fractions (FSCA) for the vegetation (Pnv represents p_{nc}) and the bare soil (Png represents p_{ng}) assuming a constant mean snowpack density of 300 kg m^{-3}. P_{nc} is shown for vegetation/surface roughness lengths varying from 0.5 to 0.05 m.

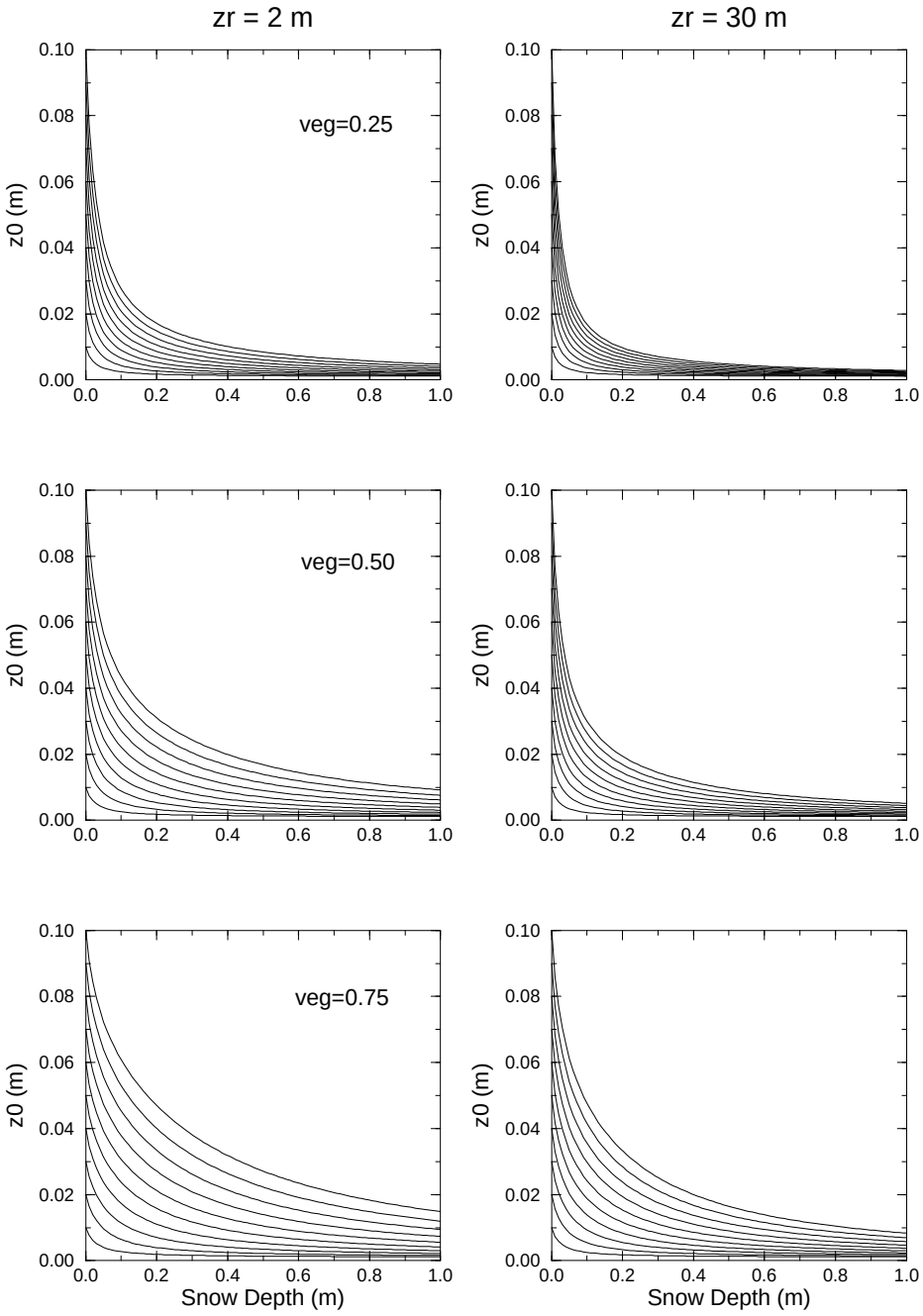

FIG. E.2. The effective surface roughness length (z_{0t}) is shown for varying values of *veg* and z_r as a function of snow depth and for varying values of the vegetation/surface roughness length (between 0.10 and 0.01 m: as in Fig. E.1).

APPENDIX F

SIMULATIONS

1. Col de Porte 1994-1995

Descriptions of the Col de Porte site (and additional references concerning this site) can be found in Boone and Etchevers (2001), Boone (2000), Essery et al. (1999) and David and Martin (1997). More details about the ISBA-ES simulation at Col de Porte can be found in Boone and Etchevers (2001).

The monthly climatology for Col de Porte for 2 years (August 1993 - July 1995) is shown in Fig. F.1 (taken from Boone and Etchevers, 2001). Results from the ISBA simulation of the snowpack for the winter of 1994-1995 (days from August 15) are shown in Fig. F.2. The simulated average snowpack density (ρ_s), snow depth (D_s) and SWE (W_s) are shown in panels a, b and c, respectively: solid lines represent the simulated values while circles are used to indicate the observed snow pit values.

The density profile ($\rho_{s\,i}$: panel d), layer thicknesses ($D_{s\,i}$: panel e) and the LWC (Liquid Water Content $W_{l\,i}$: panel f) for each of the 3 layers are also shown in Fig. F.2. The uppermost layer has the largest density fluctuations due to snowfall events (and it's relatively thin thickness), while the lowest (thickest) has the least variations (panel d). The uppermost layer was 0.05 m thick at all times except for the very beginning and end of the snow simulation. The LWC of the uppermost layer experienced a great deal of variation owing to diurnal freeze-thaw cycles. The second layer went through longer time scale cycles, while the third layer was

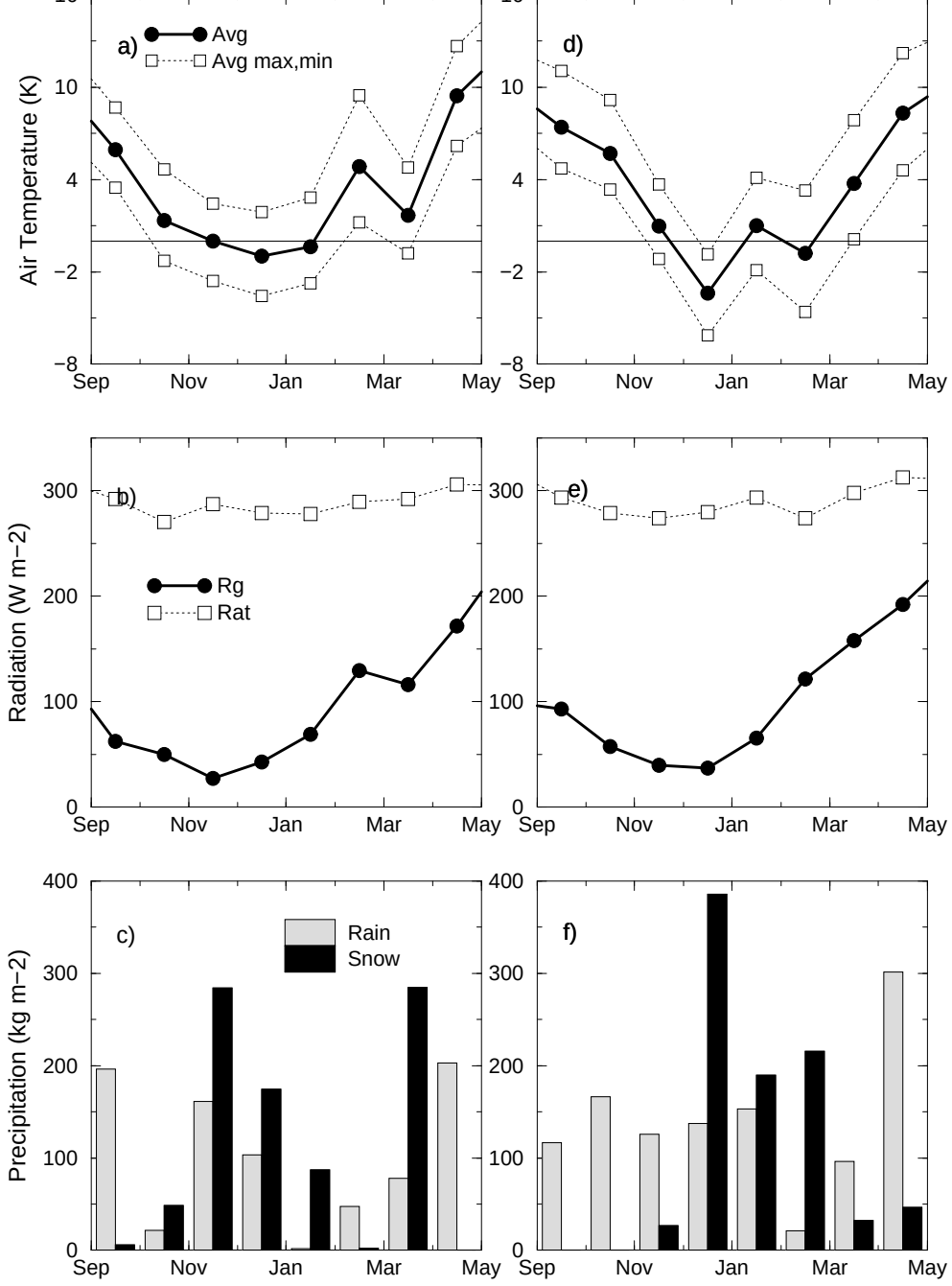

FIG. F.1. The atmospheric forcing at Col de Porte for the years 1993-1995 for the months with observed snow cover. The monthly average air temperature (T_a) is shown in panels a and d, along with the monthly average daily maximum and minimum temperatures. The atmospheric longwave (R_{at}) and incoming solar (R_g) radiation fluxes are shown in panels b and e. The monthly solid (P_n) and liquid (P_l) precipitation totals are shown in panels c and f. The labels denote the end of the month. Taken from Boone and Etchevers (2001).

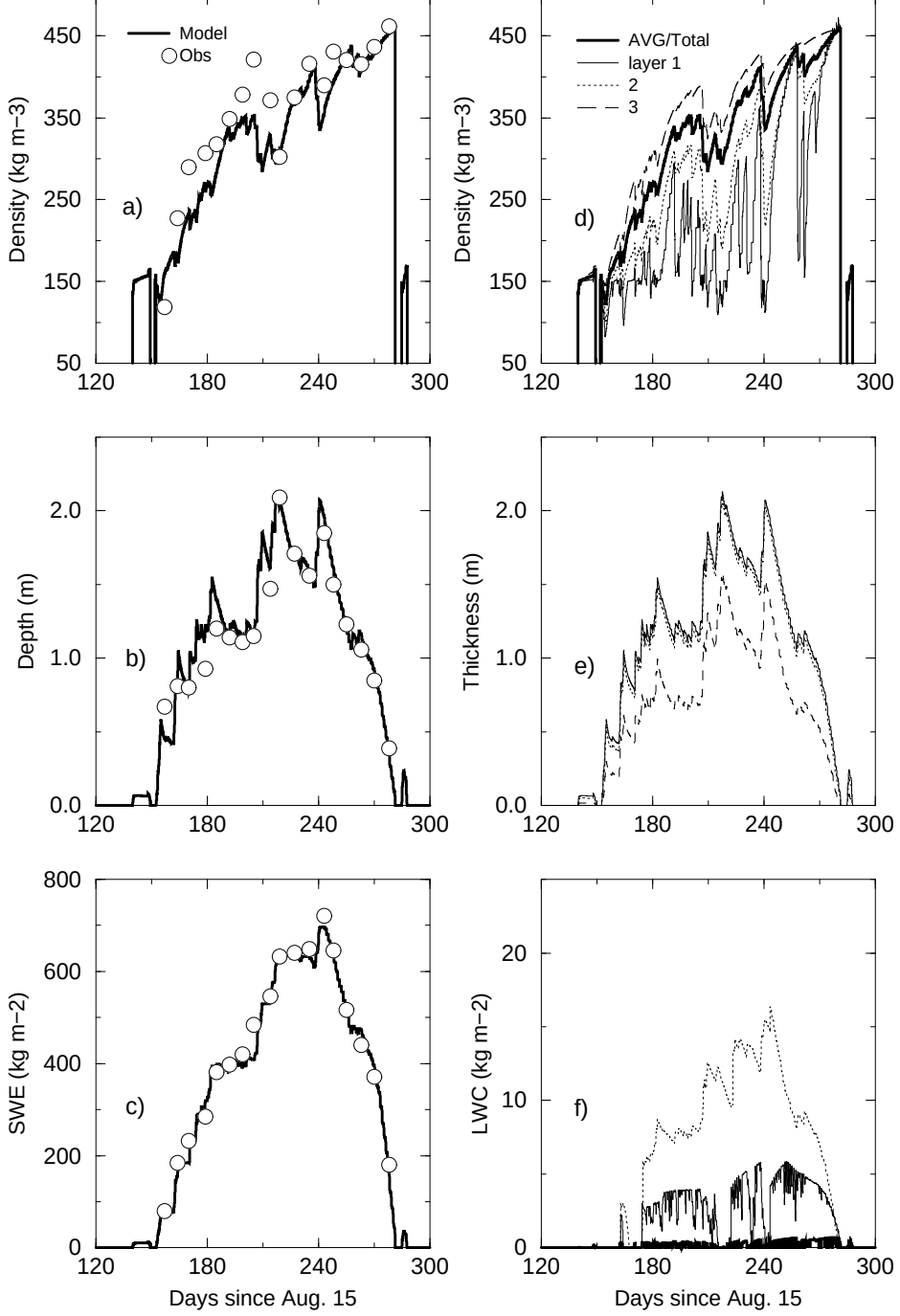

FIG. F.2. The ISBA-ES simulation of the snowpack at Col de Porte during the winter 1994-1995. The simulated average snowpack density, snow depth and SWE are shown in panels a, b and c, respectively: observations are represented by circles. The density profile (panel d), layer thicknesses (panel e) and the LWC (Liquid Water Content: panel f) for each of the 3 layers are also shown.

relatively warm and wet and experienced little refreezing during over the snow season (panel f).

The simulation of the soil temperature and moisture are shown in Fig. F.3. The explicit multi-layer soil option (Boone et al. 2000: Boone 2000) was used for this simulation. Note that because there was very limited soil freezing, the snowpack evolution is nearly identical for both the explicit multi-layer scheme and the standard force-restore approach (not shown). The soil temperature for 5 layers (thickness of 0.03, 0.12, 0.35, 0.50 and 2.00 m) is shown in panel a, while the air temperature is shown using a dotted line. All variables are shown at a 30 minute time increment. The VWC (Volumetric liquid Water Content) for the same 5 layers is shown in panel b, along with the volumetric ice content (dotted lines). Note that several mm of ice briefly formed early in the winter during a cold period when the snowpack was relatively thin: other than that period, the soil (simulated) was ice-free (which is consistent with observations at Col de Porte: see Etchevers 2000).

The snow temperature ($T_{s\,i}$) is shown for the 3-layer configuration in panel c. Successively thicker lines are used for deeper snow temperatures. Note that there is a marked diurnal freeze-thaw cycle in the uppermost layer, while the two lower layers are at the freezing point nearly all winter (due to the presence of liquid water in the snowpack). The DOS (degree of saturation) of the 3 snow layers is shown in panels d (uppermost), e (middle) and f (lowest). It is simply defined as

$$\mathrm{DOS}_i = W_{l\,i}/W_{l\,i\,\max} \qquad (0 \leq \mathrm{DOS}_i \leq 1) \quad .$$

Once again, the diurnal freeze-thaw cycle is evident in the uppermost layer (panel a), while the lowest layer is saturated for most of the duration of the snowpack (panel f). This illustrates the fact that for sites like Col de Porte in which the air temperature frequently rises above freezing, the ability to permit liquid water in the snow is necessary for a realistic thermal profile (thermal profiles and other more detailed measurements for Col de Porte can be obtained by contacting CEN: Centre Etudes de la Neige (Center for Snow Studies), Grenoble, France).

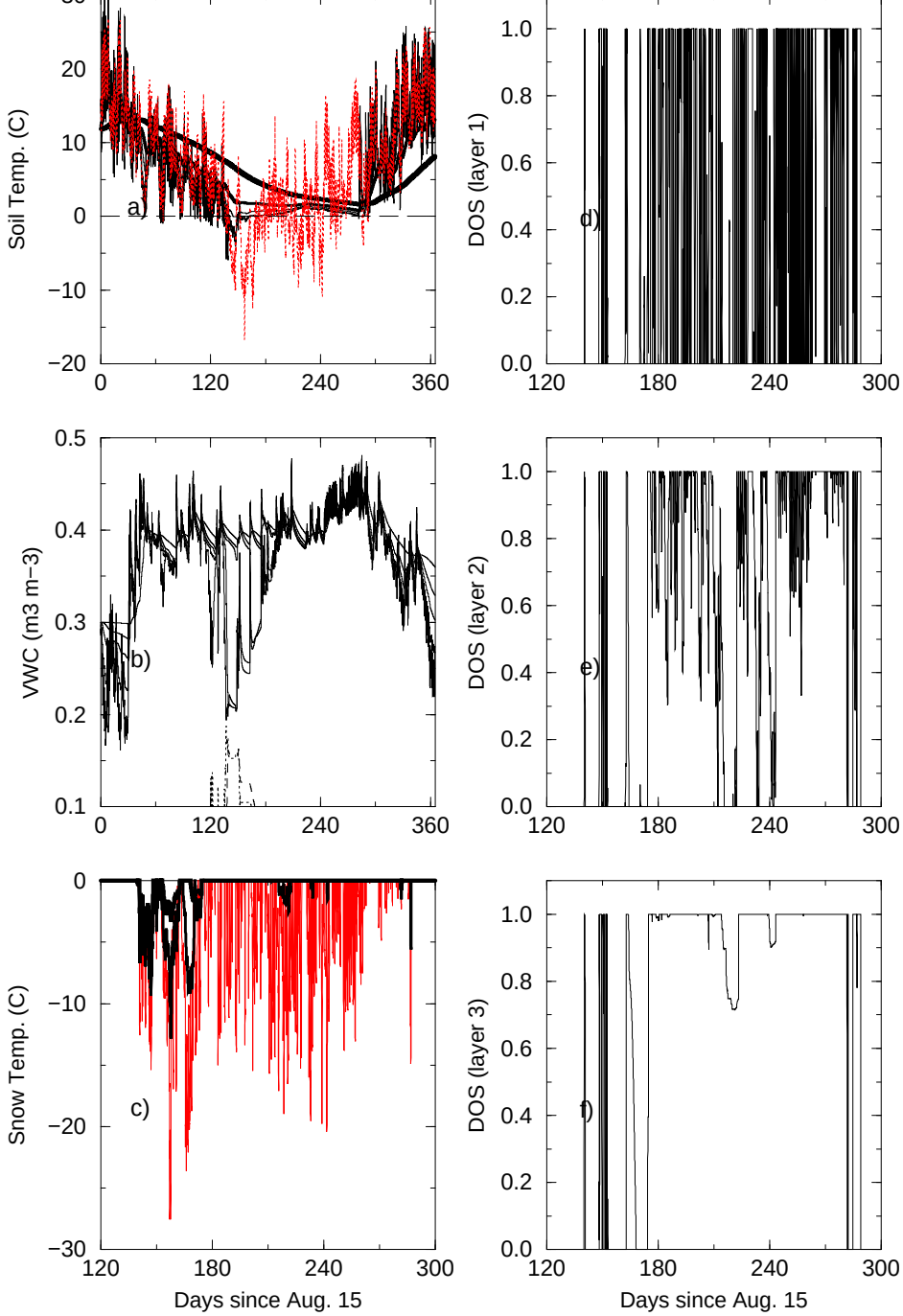

FIG. F.3. The ISBA-ES simulation of the snowpack and soil state at Col de Porte during the winter 1994-1995. The simulated soil temperature and soil moisture (liquid and ice) for 5 soil layers are shown in panels a and b, respectively. Snow temperature for 3 layers is shown in panel c. The DOS (degree of saturation of the snowpack by liquid water) is shown in panels d, e and f for layers 1, 2 and 3, respectively.

2. Rhone-AGGregation project

The Rhône aggregation Land Surface Scheme (LSS) or SVAT intercomparison project is described in Boone et al. (2001). In terms of snow model validation, the snowpack simulations from 20 simulations from 15 LSSs were compared to daily snowdepth data at 24 measurement sites within the Alps over three snow seasons (1986-1987 through 1988-1989). More details can be found in a series of forthcoming papers (Boone et al. 2002).

The Rhône basin is shown in Fig. F.4, and the 24 observations sites are indicated by the filled-red circles. The LSSs snowdepth simulations and the corresponding daily observations (averaged over all 24 sites) are shown in Fig. F.5, along with statistics (RMS=root mean square error in m, r^2=squared correlation coefficient and bias in m). Despite the difference in spatial scale between the observations (field scale) and the simulations (8x8 km grid box), some of the models were able to capture the life cycle of the snow well. For more details, see Boone et al. (2002).

The influence of the snowpack simulation on river discharge from a high altitude Alpine basin (a mean altitude of approximately 2000 m) which receives the bulk of the precipitation in the form of snow can be seen in Fig. F.6. Monthly (left column) and daily discharge statistics are shown where Eff is the efficiency or the Nash-Sutcliffe (Nash and Sutcliffe, 1970) coefficient. Only schemes with good snow depth simulations for the 6 snow-depth observation points within the Durance basin performed well in terms of simulating the discharge (which is primarily due to snowmelt). However, some schemes which simulated the snow quite well did not simulated the discharge well owing to aspects of the LSS hydrology.

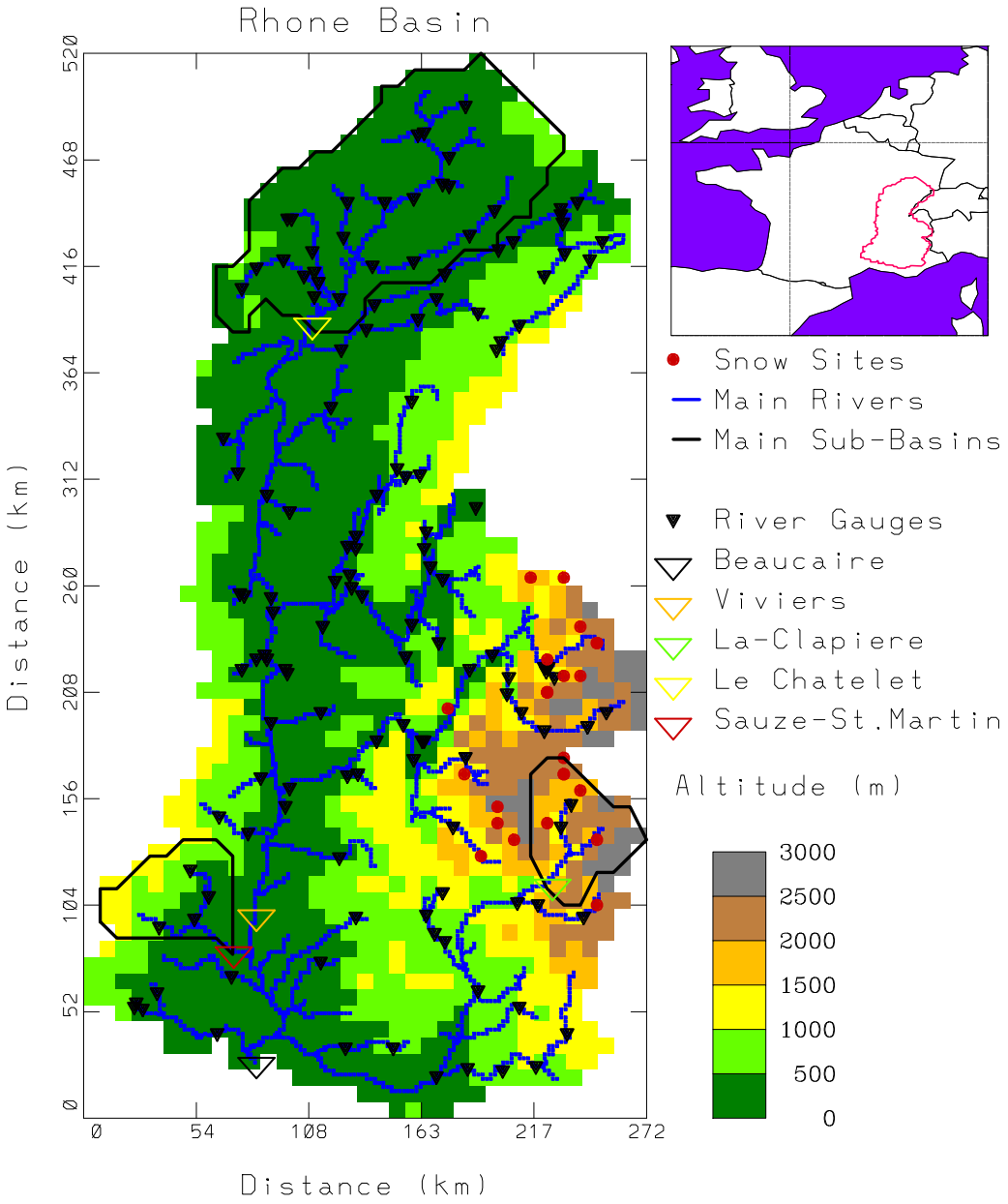

FIG. F.4. The Rhone basin used in the Rhone-AGGregation project. 24 snow observation sites are indicted using red circles. The Durance sub-basin is outlined in the south-eastern mountainous part of the domain.

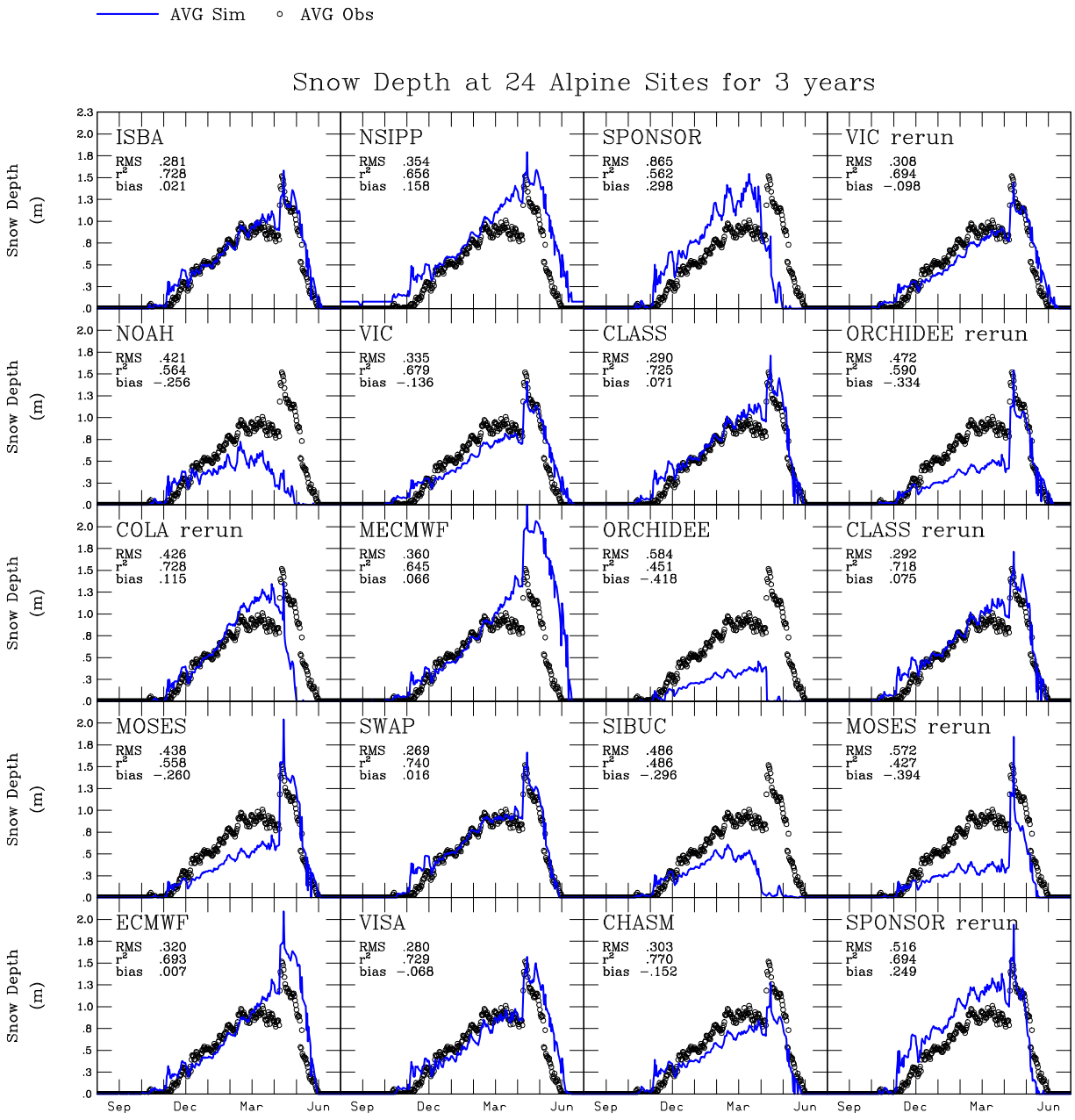

FIG. F.5. The Rhone-AGG snow simulation evaluation. The model simulated and observed snow depths averaged over 24 sites and three years are shown, along with statistics based on the daily observations. Results from ISBA-ES are shown in the upper-left corner.

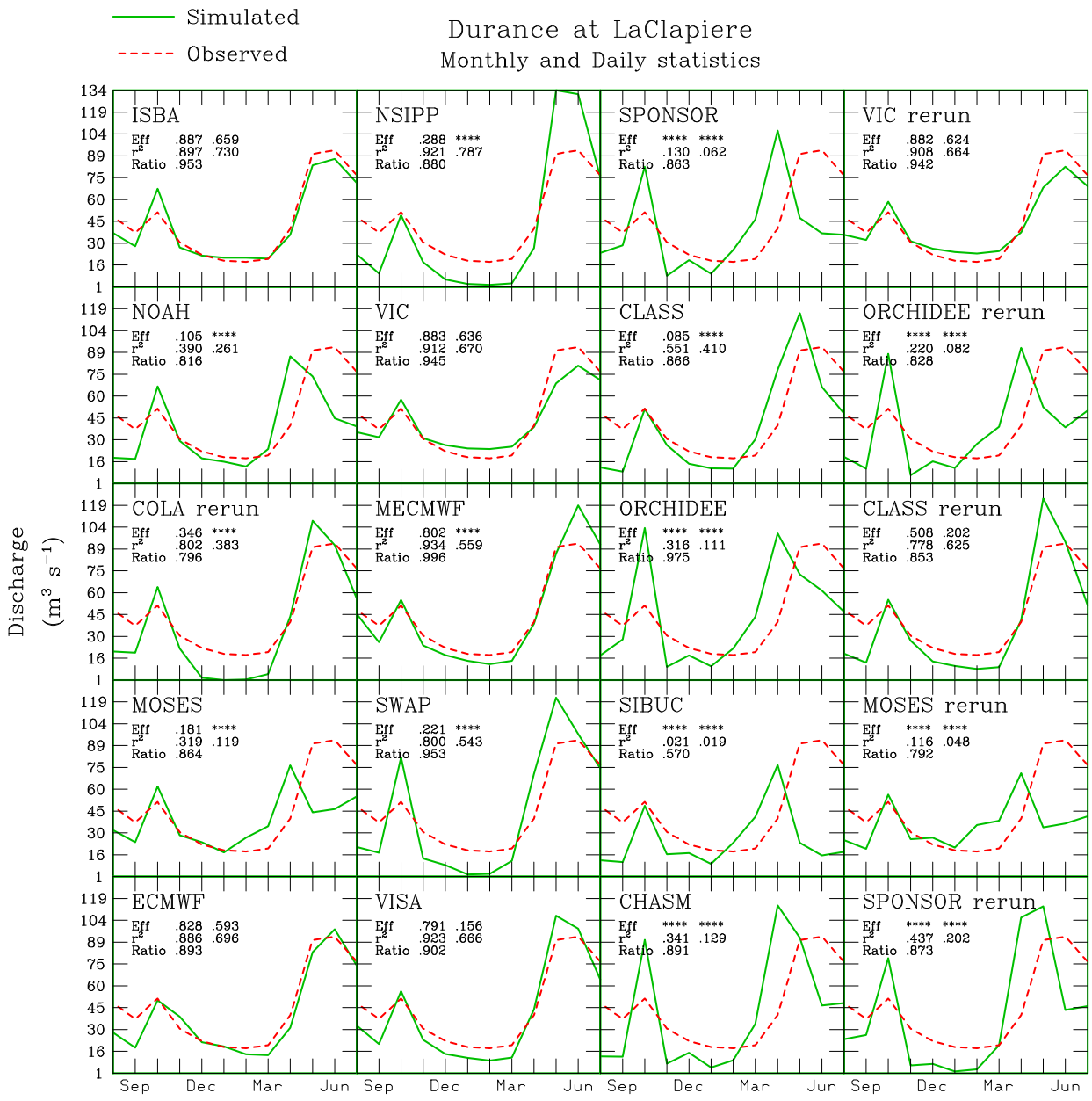

FIG. F.6. The Rhone-AGG river discharge simulation for an Alpine basin (Durance river). Monthly statistics are shown in the left column, and daily are shown in the right. The three-year average curves are shown.

REFERENCES

Anderson, E. A., 1976: A point energy and mass balance model of a snow cover. *NOAA Tech. Rep. NWS 19*, 150 pp. U.S. Dept. of Commer., Washington, D.C.

Andreas, E. L., 1996: The atmospheric boundary layer over polar marine surfaces. *CRREL, Monogr., Ser. 96-2*, Cold. Reg. Res. and Eng. Lab., Hanover, NH.

Baker, D. G., D. L. Ruschy, and D. B. Wall, 1990: The albedo decay of prairie snows. *J. Appl. Meteor.*, **29**, 179–187.

Bohren, C. F., and B. R. Barkstrom, 1974: Theory of the optical properties of snow. *J. of Geophys. Res.*, **79**(30), 4527–4535.

Boone, A., 2000: *Modélisation des processus hydrologiques dans le schéma de surface ISBA: Inclusion d'un réservoir hydrologique, inclusion du gel et modélisation de la neige* (Modeling hydrological processes in the land-surface scheme ISBA: Inclusion of a hydrological reservoir, incorporation of soil ice and snow modeling). Ph.D. Thesis, Univ. Paul Sabatier, Toulouse, France.

——, V. Masson, T. Meyers, and J. Noilhan, 2000: The influence of the inclusion of soil freezing on simulations by a soil-vegetation-atmosphere transfer scheme. *J. Appl. Meteor.*, **9**, 1544–1569.

——, and P. Etchevers, 2001: An intercomparison of three snow schemes of varying complexity coupled to the same land-surface scheme. Local scale evaluation at an Alpine site. *J. Hydrometeor.*, **2**, 374–394.

——, F. Habets, J. Noilhan, 2001: The Rhone-AGGregation Experiment. *GEWEX News*, WCRP, **11**(3), 3–5.

——, F. Habets, J. Noilhan, E. Blyth, D. Clark, P. Dirmeyer, Y. Gusev, I. Haddeland, R. Koster, D. Lohmann, S. Mahanama, K. Mitchell, O. Nasonova, G.-Y. Niu, A. Pitman, J. Polcher, A. B. Shmakin, K. Tanaka, B. van den Hurk, S. Verant, D. Verseghy, and P. Viterbo, 2002: The Rhone-AGGregation Land Surface Scheme Intercomparison Project: An Overview. *J. Climate*, **17**, 187–208.

Bowling, L. C., D. P. Lettenmaier, B. Nijssen, L. P. Grahm, D. B. Clark, M. El Maayar, R. Essery, S. Goers, F. Habets, B. van den Hurk, J. Jin, D. Kahan, D. Lohmann, S. Mahanama, D. Mocko, O. Nasonova, A. Shmakin, D. Verseghy, P. Viterbo, Y. Xia, X. Ma, Y. Xue, and Z.-L. Yang, 2002: Simulation of high latitude hydrological processes in the Torne-Kalix basin: PILPS Phase-2(e), 1: Experiment description and summary intercomparisons. *Global and Plan. Change*, **38**, 1–30.

Brun, E., E. Martin, V. Simon, C. Gendre, C. Coleou, 1989: An energy and mass balance model of snow cover suitable for operational avalanche forecasting. *J. Glaciol.*, **35**, 333–342.

——, P. David, M. Sudul, and G. Brunot, 1992: A numerical model to simulate snow cover stratigraphy for operational avalanche forecasting. *J. Glaciol.*, **38**, 13–22.

——, E. Martin, V. Spiridonov, 1997: The coupling of a multi-layered snow model with a GCM. *Ann. Glaciol.*, **25**, 66–72.

David, P., and E. Martin, 1997: Le laboratoire du Col de Porte: historique et climatologie. Centre d'Etudes de la Neige Note 9, St. Martin d'Hères, France.

Derbyshire, S. H., 1999: Boundary-layer decoupling over cold surfaces as a physical boundary-instability. *Bound.–Layer Meteor.*, **90**, 297–325.

Dickinson, R. E., 1988: The force-restore model for surface temperatures and its generalizations. *J. Climate*, **1**, 1086–1097.

Douville, H., Royer J.-F., Mahfouf, J.-F., 1995: A new snow parameterization for the Météo-France climate model. Part 1: validation in stand-alone experiments. *Clim. Dyn.*, **12**, 21–35.

Essery, R., E. Martin, H. Douville, A. Fernández, and E. Brun, 1999: A comparison of four snow models using observations from an alpine site. *Clim. Dyn.*, **15**, 583–593.

Etchevers, P., 2000: *Modélization du cycle continental de l'eau á l'échelle régional: Impact de la modélization de l'enneigement sur l'hydrologie du bassin versant du Rhône.* (Modeling the continental water cycle at a regional scale: Impact of the snow simulation on the hydrology of the Rhone basin.) Ph.D. Thesis, Univ. Paul Sabatier, Toulouse, France.

Giordani, H., 1993: *Description du codage du schema de surface NP89 aux normes ARPEGE: Premieres Validations.* Note Trav. **15**, GMME/Météo-France, 62 pp.

Girard, G., 1974: Modèle global ORSTOM. Première application du modèle jornalier à discretisation spatiale sur le bassin versant de la crique Grégoire en guyane. Technical report, ORSTOM, Paris. Atelier hydrologique sur les modèles mathématiques.

Hardy, J. P., R. E. Davis, R. Jordan, X. Li, C. Woodcock, W. Ni, and J. C. McKenzie, 1997: Snow ablation modeling at the stand scale in a boreal jack pine forest. *J. of Geophys. Res.*, **102**, 29,397–29,405.

Jordan, R., 1991: A one-dimensional temperature model for a snow cover. *CRREL, Special Report 91-1b*, Cold. Reg. Res. and Eng. Lab., Hanover, NH.

——, E. L. Andreas, and A. P. Makshatas, 1999: Heat budget of snow-covered sea ice at North Pole 4. *J. of Geophys. Res.*, **104**, 7785–7806.

Kojima, K., 1967: Densification of a seasonal snow cover, Physics of Snow and Ice, *Proc. Int. Conf. Low Temp. Sci.*, **1**(2), S.929–S.952.

Kondo, J., and H. Yamazaki, 1990: A prediction model for snow melt, snow surface temperature and freezing depth using a heat balance method. *J. Appl. Meteor.*, **29**, 375–384.

Koren, V., J. Schaake, K. Mitchell, Q.-Y. Duan, F. Chen and J. M. Baker, 1999: A parameterization of snowpack and frozen ground intended for NCEP weather and climate models. *J. of Geophys. Res.*, **104**, 19,569–19,585.

Krinner, G., C. Genthon, Z.-X. Lin, and P. Le Van, 1997: Studies of the Antarctic climate with a stretched grid general circulation model. *J. of Geophys. Res.*, **102**, 13731–13745.

Ledoux, E., G. Girard, G. de Marsilly, J. Deschenes, 1989: Spatially distributed modeling: conceptual approach, coupling surface water and ground water, NATO, ASI Series C. In: Morel-Seytoux, X. (Ed.). Unsaturated Flow Hydrologic Modeling-theory and Practice, 275 pp. Kluwer Academic, Dordrecht pp. 435–454.

Loth, B., H.-F. Graf, and J. M. Oberhuber, 1993: Snow cover model for global climate simulations. *J. of Geophys. Res.*, **98** (D6), 10,451–10,464.

——, and H.-F. Graf, 1998: Modeling the snow cover in climate studies. Part 1: Long-term integrations under different climatic conditions using a multi-layered snow-cover model. *J. of Geophys. Res.*, **103**, 11,313–11,327.

Louis, J. F., 1979: A parametric model of vertical eddy fluxes in the atmosphere. *Bound.–Layer Meteor.*, **17**, 187–202.

Lynch-Stieglitz, M., 1994: The development and validation of a simple snow model for the GISS GCM. *J. Climate*, **7**, 1842–1855.

Marks, D., and A. Winstral, 2001: Comparison of snow deposition, the snow cover energy balance, and snowmelt at two sites in a semiarid mountain basin. *J. Hydrol.*, **2**, 213–227.

Martin, E., and Y. Lejeune, 1998: Turbulent fluxes above the snow surface. *Ann. Glaciol.*, **26**, 179–183.

Mellor, M., 1964: Properties of snow, *Cold Reg. Sci. Eng. Monogr. III-A1*, 105 pp.

Nash, J. E., and J. V. Sutcliffe, 1970: River flow forecasting through conceptual models, 1, a discussion of principles. *J. Hydrol.*, **10**(3), 282–290.

Nijssen, B., Bowling, L. C., D. P. Lettenmaier, D. B. Clark, M. El Maayar, R. Essery, S. Goers, F. Habets, B. van den Hurk, J. Jin, D. Kahan, D. Lohmann, S. Mahanama, D. Mocko, O. Nasonova, P. Samuelsson, A. Shmakin, K. Takata, D. Verseghy, P. Viterbo, Y. Xia, X. Ma, Y. Xue, and Z.-L. Yang, 2002: Simulation of high latitude hydrological processes in the Torne-Kalix basin: PILPS Phase-2(e), 2: Comparison of model results with observations. *Global and Plan. Change*, **38**, 31–53..

Noilhan, J. and S. Planton, 1989: A simple parameterization of land surface processes for meteorological models. *Mon. Wea. Rev.*, **117**, 536–549.

——and J.-F. Mahfouf, 1996: The ISBA land surface parameterization scheme. *Global and Plan. Change*, **13**, 145–159.

Pitman, A. J., Z-L. Yang, J. G. Cogley and A. Henderson-Sellers, 1991: Description of bare essentials of surface transfer for the bureau of meteorology research centre AGCM. *BMRC Research Report No. 32*, various pagings.

Schlosser, C. A., A. G. Slater, A. Robock, A. J. Pitman, K. Y. Vinnkov, A. Henderson-Sellers, N. A. Speranskaya, K. Mitchell, A. Boone, H. Braden, F. Chen, P. Cox, P. de Rosnay, C. E. Desborough, R. E. Dickinson, Y.-J. Dai,

Q. Duan, J. Entin, P. Etchevers, N. Gedney, Y. M. Gusev, F. Habets, J. Kim, V. Koren, E. Kowalczyk, O. N. Nasonova, J. Noilhan, J. Schaake, A. B. Shmakin, T. G. Smirnova, D. Verseghy, P. Wetzel, Y. Xue, and Z.-L. Yang, 2000: Simulations of a boreal grassland hydrology at Valdai, Russia: PILPS Phase 2(d). *Mon. Wea. Rev.*, **128**, 301–321.

Slater, A. G., A. J. Pitman, and C. E. Desborough, 1998: The validation of a snow parameterization designed for use in general circulation models. *Int. J. Climatol.*, **18**, 595–617.

——, C. A. Schlosser, C. E. Desborough, A. J. Pitman, A. Henderson-Sellers, A. Robock, Y. Vinnkov, K. Mitchell, A. Boone, H. Braden, F. Chen, P. Cox, P. de Rosnay, R. E. Dickinson, Y.-J. Dai, Q. Duan, J. Entin, P. Etchevers, N. Gedney, Y. M. Gusev, F. Habets, J. Kim, V. Koren, E. Kowalczyk, O. N. Nasonova, J. Noilhan, J. Schaake, A. B. Shmakin, T. G. Smirnova, D. Verseghy, P. Wetzel, Y. Xue, and Z.-L. Yang, 2001: Simulations of a boreal grassland hydrology at Valdai, Russia: The Representation of Snow in Land-surface Schemes ; results from PILPS 2(d). *J. Hydrometeor.*, **2**, 7–25.

Sud, Y. C., and D. M. Mocko, 1999: New snow-physics to complement SSiB, Part I: Design and evaluation with ISLSCP initiative I datasets. *J. Meteor. Soc. Japan*, **77**(1B), 335–348.

Sun, S., J. Jin, and Y. Xue, 1999: A simple snow-atmosphere-soil transfer (SAST) model. *J. of Geophys. Res.*, **104**, D16, 19587–19579.

Verseghy, D. L., 1991: CLASS - A Canadian land surface scheme for GCMs. I. Soil Model. *Int. J. Climatol.*, **11**, 111–133.

Viterbo, P., A. Beljaars, J.-F. Mahfouf, and J. Teixeira, 1999: The representation of soil moisture freezing and its impact on the stable boundary layer. *Q. J. R. Meteorol. Soc.*, **125**, 2401–2426.

Yang, Z.-L., R. E. Dickinson, A. Robock, and K. Y. Vinnikov, 1997: Validation of snow sub-model of the biosphere-atmosphere transfer scheme with Russian snow-cover and meteorological observations data. *J. Climate*, **10**, 353–373.